2m14

ELECTRICAL

ENGINEERING

ENGINEERING EXPERIMENT STATION

AUBURN UNIVERSITY

AUBURN, ALABAMA

SOME OPTIMAL CONSIDERATIONS IN ATTITUDE CONTROL SYSTEMS

PREPARED BY

GUIDANCE AND CONTROL STUDY GROUP

JOSEPH S. BOLAND, III, PROJECT LEADER

THIRD TECHNICAL REPORT

SEPTEMBER 14, 1973

CONTRACT NAS8-26580
GEORGE C. MARSHALL SPACE FLIGHT CENTER
NATIONAL AERONAUTICS AND SPACE ADMINISTRATION
HUNTSVILLE, ALABAMA

APPROVED BY:

J. David Irwin
Associate Professor and Head
Electrical Engineering

SUBMITTED BY:

Joseph S. Boland, III
Associate Professor
Electrical Engineering

FOREWORD

This report is a technical summary of the progress made by the Electrical Engineering Department, Auburn University, toward fulfillment of Contract NAS8-26580 granted to Auburn Research Foundation, Auburn, Alabama. This contract was awarded November 15, 1970, by the George C. Marshall Space Flight Center, National Aeronautics and Space Administration, Huntsville, Alabama.

PERSONNEL

The following staff members of the Electrical Engineering Department of Auburn University have actively participated in the work of this contract:

J. S. Boland, III - Associate Professor and Project Leader

B. K. Colburn - Graduate Research Assistant

D. M. Drinkard - Graduate Research Assistant

L. R. White - Graduate Research Assistant

SUMMARY

The conventional six-engine reaction control jet relay attitude control law with deadband is shown to be a good linear approximation to a weighted time-fuel optimal control law. Techniques for evaluating the value of the relative weighting between time and fuel for a particular relay control law is studied along with techniques to interrelate other parameters for the two control laws.

Vehicle attitude control laws employing control moment gyros are then investigated. Steering laws obtained from the expression for the reaction torque of the gyro configuration are compared to a total optimal attitude control law that is derived from optimal linear regulator theory. This total optimal attitude control law has computational disadvantages in the solving of the matrix Riccati equation. Several computational algorithms for solving the matrix Riccati equation are investigated with respect to accuracy, computational storage requirements, and computational speed.

TABLE OF CONTENTS

LIST OF TABLES

LIST OF FIGURES

I. INTRODUCTION

Some aspects of optimal attitude control systems are examined in this study. The conventional six-engine reaction control jet relay attitude control law with deadband is compared to an optimal weighted time-fuel attitude control law. The relay attitude control is shown to be a good linear approximation to the weighted time-fuel optimal control law, then a procedure is developed to determine the optimal control law weighting of time and fuel that corresponds to a given relay attitude control law with deadband. This time-fuel weighting value is determined by selecting the value that minimizes the mean square error between the switching curves of the two control laws. Next, a procedure is developed to determine the six-engine relay attitude control law with deadband that most closely corresponds to a given optimal weighted time-fuel attitude control law.

Vehicle attitude control laws employing control moment gyros (CMGs) are then investigated. The reaction torque of the gyro configuration on the vehicle is determined in terms of the gimbal angles, the gimbal rates, and the vehicle rates. This expression cannot be solved for the gimbal rates directly, so different procedures for obtaining the gimbal rates are examined. Basic approaches to obtaining these steering laws given the commanded torque are compared with an optimal control moment gyro attitude control law that is obtained

from optimal linear regulator theory. This system is reduced to the linear regulator by frequently linearizing the system as the CMG gimbal angles travel some prescribed amount from their previous nominal value. This total optimal CMG attitude control law has some computational disadvantages in attempting to solve the matrix Riccati equation on a flight control computer. A sensitivity analysis is performed on the gain matrix to determine if any gains can be considered constant. Several computational algorithms for solving the Riccati equation are investigated with respect to accuracy, computational storage requirements, and computational speed.

II. RELATION OF A REACTION CONTROL JET CONTROL LAW TO AN OPTIMAL WEIGHTED TIME-FUEL CONTROL LAW

The attitude control law for the conventional six engine reaction control jet system has the phase plane portrait shown in Figure II-1. Although it is suspected that this control law was originally developed empirically, it will be shown that this law closely approximates one determined by utilizing optimal control procedures.

The analysis will be simplified by assuming that the system dynamics can be represented as $1/s^2$. It will also be assumed that the position, ϕ, can be obtained by integrating the body rate, $\dot{\phi}$, directly and that the position and rate signals can be measured. With these simplifications, the system to be controlled is depicted in Figure II-2. The state equations for this single-axis system are

$$\begin{aligned} \dot{x}_1 &= x_2 \\ \dot{x}_2 &= u \end{aligned} \tag{II-1}$$

For a reaction control jet control system, the elements to be considered in a performance measure are time, fuel, and final state. The performance measure will not penalize the final state, but rather the final state will be constrained to lie within the deadzone limits (i.e., $|\phi(t_f)| \leq \phi_{dB}$). Thus, the performance measure weighting time and fuel is

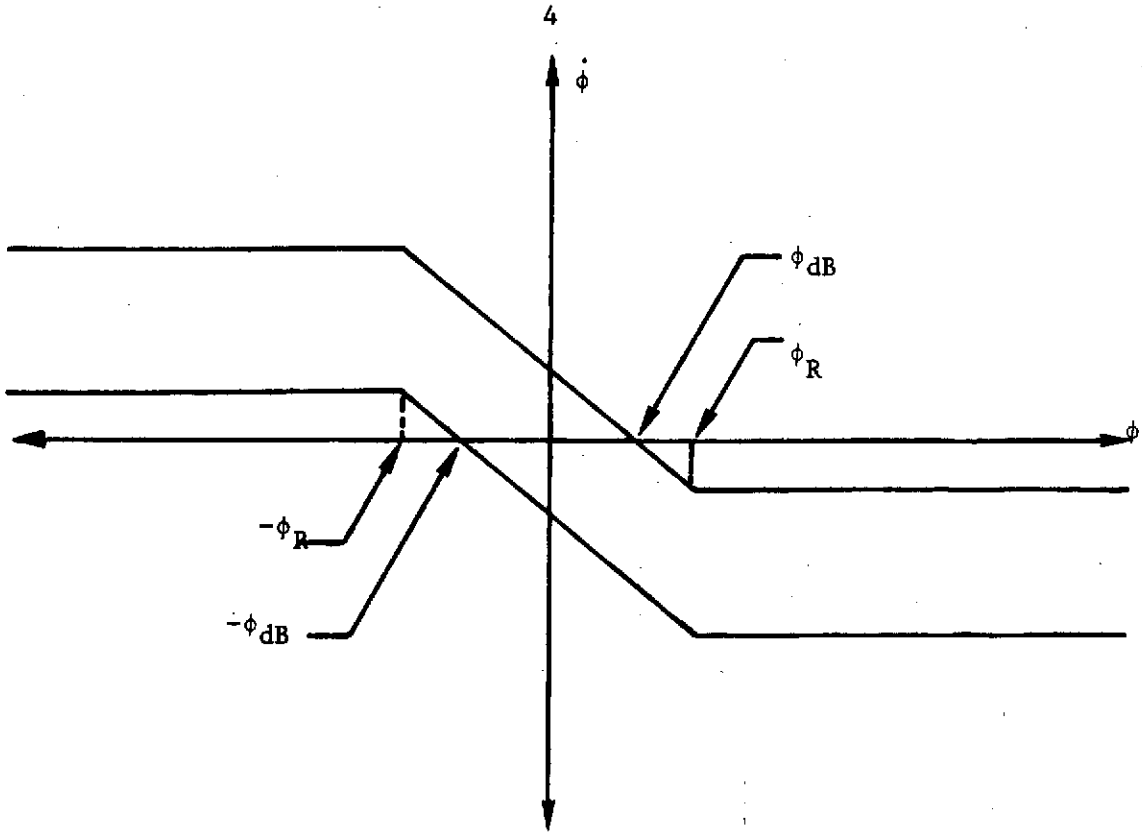

Figure II-1. Phase-plane portrait of six-engine reaction control jet attitude control law.

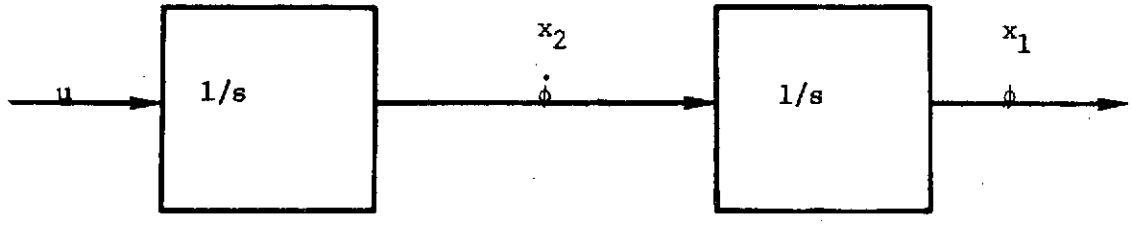

Figure II-2. Open loop simplified system to be controlled.

$$J(u) = \int_{t_o}^{t_f} \left\{ \lambda + |u(t)| \right\} dt \qquad \text{(II-2)}$$

where λ is the relative weighting of time and fuel, and u(t) is the control law. Since the final position is constrained to lie within the deadzone limits, this problem can be solved for $\phi(t_f) = 0$ and the results shifted to the limits $\phi(t_f) = \phi_{dB}$ and $\phi(t_f) = -\phi_{dB}$ for the solution to the deadzone problem.

For this problem, the Hamiltonian is

$$H = \lambda + |u| + p_1 x_2 + p_2 u \qquad \text{(II-3)}$$

The necessary conditions for optimality are

$$\frac{\partial H}{\partial p_1} = \dot{\hat{x}}_1 = \hat{x}_2 \qquad \text{(II-4)}$$

$$\frac{\partial H}{\partial p_2} = \dot{\hat{x}}_2 = \hat{u} \qquad \text{(II-5)}$$

$$-\frac{\partial H}{\partial x_1} = \dot{\hat{p}}_1 = 0 \qquad \text{(II-6)}$$

$$-\frac{\partial H}{\partial x_2} = \dot{\hat{p}}_2 = -\hat{p}_1 \qquad \text{(II-7)}$$

$$|\hat{u}| + \hat{p}_2 \hat{u} \leq |u| + \hat{p}_2 u \qquad \text{(II-8)}$$

where the hat above the states, costates, and control indicates the optimal trajectories and the optimal control history. Pontryagin's minimum principle, Equation (II-8), reveals that the form of the optimal

control is

$$\hat{u} = \begin{cases} +1 & \text{for } \hat{p}_2 < -1 \\ 0 & \text{for } -1 < \hat{p}_2 < 1 \\ -1 & \text{for } \hat{p}_2 > 1 \\ \text{singular} & \text{for } \hat{p}_2 = \pm 1 \end{cases} \qquad \text{(II-9)}$$

Integrating Equations (II-6) and (II-7) yields the following solutions to the costate equations

$$\begin{aligned} \hat{p}_1 &= C_1 \\ \hat{p}_2 &= -C_1 t + C_2 \end{aligned} \qquad \text{(II-10)}$$

where C_1 and C_2 are constants of integration. The solution for $\hat{p}_2$ indicates two things about the optimal control since $\hat{u}$ is expressed as a function of the costate trajectory, $\hat{p}_2$. First, singular control exists only for the special case with $C_1=0$ and $C_2=\pm 1$. If C_1 is any value other than zero, $\hat{p}_2$ cannot remain at ± 1 for any finite period of time. For $C_1=0$, $\hat{p}_2=C_2$ indicating the condition that $C_2=\pm 1$ for the existence of singular control. Secondly, for $C_1 \neq 0$, $\hat{p}_2$ changes sign no more than once (at $t=C_2/C_1$) and passes through $\hat{p}_2=-1$ and $\hat{p}_2=+1$ no more than once, resulting in two control switchings at most. This indicates that the form of the optimal control law in its most general form will be $\{1,0,-1\}$ or $\{-1,0,1\}$. Depending on the initial conditions, the first elements in these control strategies might be unnecessary. These special case control strategies are $\{0,-1\}$, $\{0,1\}$, $\{-1\}$, and $\{1\}$.

Integrating Equation (II-5) with $\hat{u}=\pm 1$ yields the solution for $\hat{x}_2$ as

$$\hat{x}_2 = \pm t + C_3 \tag{II-11}$$

where C_3 is a constant of integration. Then integrating Equation (II-4) yields

$$\hat{x}_1 = \pm\tfrac{1}{2}t^2 + C_3 t + C_4 \tag{II-12}$$

where C_4 is a constant of integration. Solving Equation (II-11) for t and substituting this result into the expression for $\hat{x}_1$ given by Equation (II-12) gives the trajectories in the phase plane for $u=\pm 1$ as

$$\hat{x}_1 = \pm\tfrac{1}{2}\hat{x}_2^2 + C_5 \tag{II-13}$$

where $C_5 = C_4 - \tfrac{1}{2} C_3^2$ for $u = +1$

and $C_5 = C_4 + \tfrac{1}{2}C_3^2$ for $u = -1$

Integrating Equation (II-5) when $\hat{u}=0$ reveals that $\hat{x}_2$ is simply a constant for any such period in the optimal control history. Then, integrating Equation (II-4) yields

$$\hat{x}_1 = k_1 t + k_2 \tag{II-14}$$

where k_1 and k_2 are the constants of integration. Therefore, when $\hat{u}=0$, $\hat{x}_2$ remains constant and $\hat{x}_1$ increases or decreases with time depending on the value of $\hat{x}_2$ at the time $\hat{u}$ is switched to zero.

The parabolas defined by Equation (II-13) for $C_5=0$ are the minimum time switching curves that will bring the system into the origin of the phase plane. The remaining step is to determine the switching lines that define the switch from $\hat{u}=-1$ to $\hat{u}=0$ and the switch from $\hat{u}=+1$ to $\hat{u}=0$. Following the procedure employed by Kirk [1], t_o denotes the time when the optimal control switches from +1 to 0 and t_1 denotes the time when the optimal control switches from 0 to -1. Figure II-3 shows some candidate trajectories for a given initial condition. Since t_o occurs somewhere on the segment C-K, points D, F, and H are candidate points on the switching curve that switches $\hat{u}$ from +1 to 0. The points E, G, and I are corresponding candidate switching points for the switch from 0 to -1 since t_1 must occur on the segment K-0. Equation (II-13) relates $\hat{x}_1$ and $\hat{x}_2$ on K-0, so that

$$\hat{x}_1(t) = -\tfrac{1}{2}\hat{x}_2^2(t), \tag{II-15}$$

which leads to

$$\hat{x}_1(t_1) = -\tfrac{1}{2}\hat{x}_2^2(t_1) \quad . \tag{II-16}$$

Integrating Equation (II-5) with $\hat{u}=0$, for the switch from $\hat{u}=+1$ to $\hat{u}=0$ occurring at $t=t_o$, yields

$$\hat{x}_2(t) = k_3 = \hat{x}(t_o) \tag{II-17}$$

Then, integrating Equation (II-4) gives

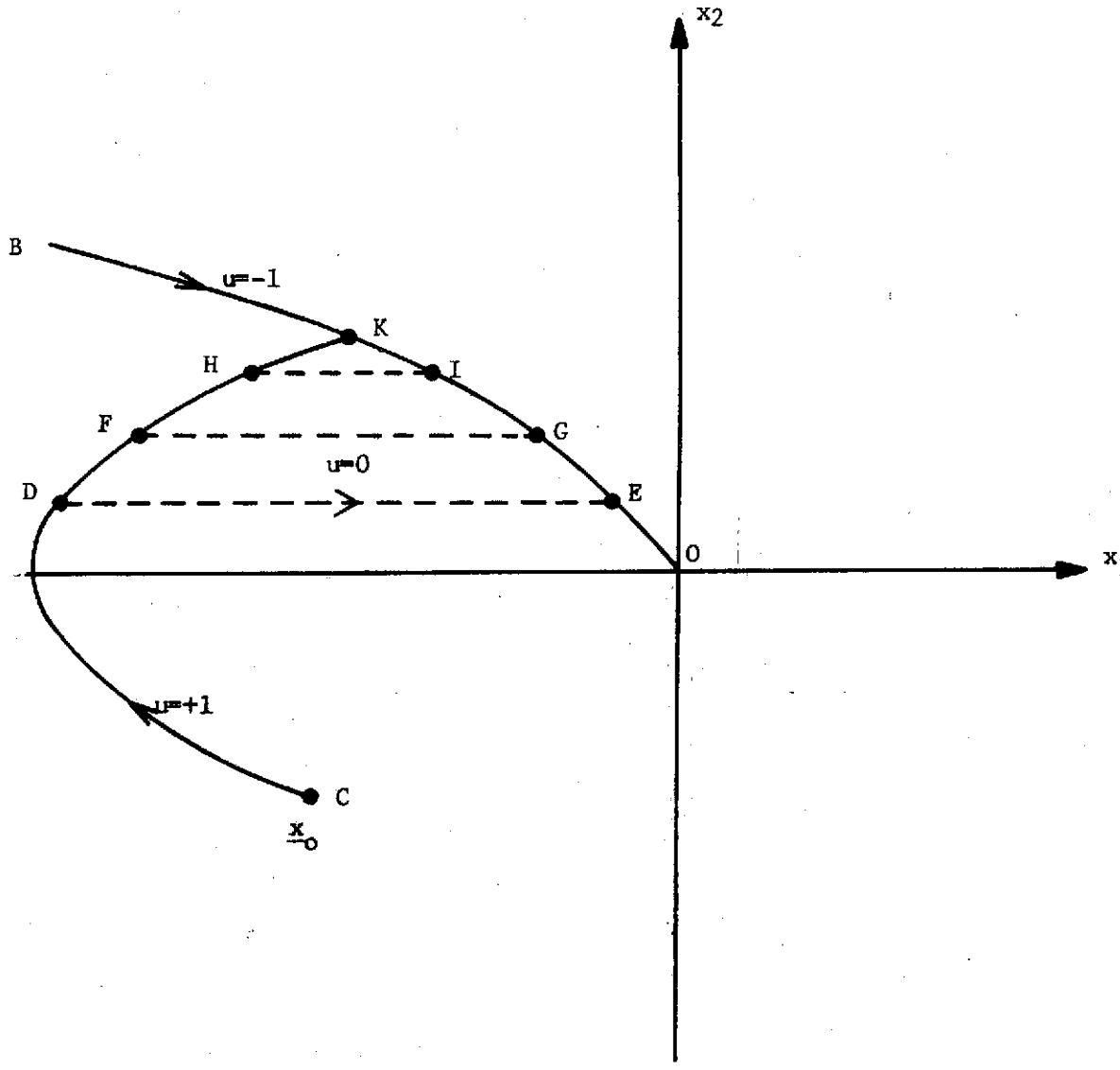

Figure II-3. Some candidates for the optimal trajectory with initial conditions $x_1(0) = x_{10}$ and $x_2(0) = x_{20}$.

$$\int_{t_o}^{t_1} \dot{\hat{x}}_1(t)dt = \int_{t_o}^{t_1} \hat{x}_2(t_o)dt \qquad \text{(II-18)}$$

Therefore, performing the integration of (II-18) yields

$$\hat{x}_1(t_1) = \hat{x}_1(t_o) + \hat{x}_2(t_o)[t_1 - t_o] \qquad \text{(II-19)}$$

As was earlier determined using Pontryagin's minimum principle, $\hat{p}_2=\pm 1$ for control switchings. Using this result in Equations (II-10) yields

$$\hat{p}_2(t_o) = -C_1 t_o + C_2 = -1 \qquad \text{(II-20)}$$

$$\hat{p}_2(t_1) = -C_1 t_1 + C_2 = 1 \qquad \text{(II-21)}$$

Since $\hat{x}_2(t)$ is a constant for $\hat{u}=0$, then $\hat{x}_2(t_o) = \hat{x}_2(t_1)$. Since the Hamiltonian is required to be identically zero along the optimal trajectory, at $t=t_o$

$$\lambda + |\hat{u}(t_o)| + C_1\hat{x}_2(t_o) + \hat{p}_2(t_o)\hat{u}(t_o) = 0 \qquad \text{(II-22)}$$

but
$$|\hat{u}(t_o)| + \hat{p}_2(t_o)\hat{u}(t_o) = 0 \qquad \text{(II-23)}$$

since $\hat{p}_2(t_o) = -1$. Therefore,

$$\lambda + C_1\hat{x}_2(t_o) = 0 \qquad \text{(II-24)}$$

Solving Equation (II-24) for C_1 gives

$$C_1 = -\frac{\lambda}{\hat{x}_2(t_o)} \tag{II-25}$$

Subtracting Equation (II-21) from Equation (II-20) yields

$$[t_1 - t_o] = -2/C_1 \quad , \tag{II-26}$$

which, using Equation (II-25), becomes

$$[t_1 - t_o] = \frac{2\hat{x}_2(t_o)}{\lambda} \tag{II-27}$$

Equating the expressions for $\hat{x}_1(t_1)$ given by Equations (II-16) and (II-19) gives

$$-\tfrac{1}{2}\hat{x}_2^2(t_1) = -\tfrac{1}{2}\hat{x}_2^2(t_o) = \hat{x}_1(t_o) + \hat{x}_2(t_o)[t_1 - t_o] \tag{II-28}$$

Using Equation (II-27), Equation (II-28) becomes

$$-\tfrac{1}{2}\hat{x}_2^2(t_o) = \hat{x}_1(t_o) + \frac{2\hat{x}_2^2(t_o)}{\lambda} \tag{II-29}$$

which can be solved for $\hat{x}_1(t_o)$ to give the switching line in the phase plane as

$$\hat{x}_1(t_o) = -\frac{\lambda+4}{2\lambda}\,\hat{x}_2^2(t_o) \tag{II-30}$$

In an analogous manner the switching curve for $\hat{u}=-1$ to $\hat{u}=0$ is determined to be

$$\hat{x}_1(t_o) = \frac{\lambda+4}{2\lambda}\,\hat{x}_2^2(t_o) \qquad \text{(II-31)}$$

Figure II-4 shows several of these optimal switching curves for various values of λ. These results confirm the intuitive feeling that as λ approaches infinity the weighted time-fuel law approaches the minimum time control law. Figure II-5 shows some weighted time-fuel optimal trajectories for three sets of initial conditions with $\lambda=1$.

Now, to analyze the original deadzone problem, these results will be shifted to $\phi(t_f) = \phi_{dB}$ and $\phi(t_f) = -\phi_{dB}$ by a change of variables. The phase plane portrait that is obtained by this shift is shown in Figure II-6. However, since the control law only maintains ϕ within a deadband, then the inner switching curves are meaningless. The internal λ switching curves, B-F and C-G, will be omitted because another of the switching curves has preceded these curves in performing its originally intended switching function. The internal minimum time optimal switching curves, A-B-C and F-G-H, could possibly be used along with the external switching curves, I-C-D and E-F-J. They are omitted because any overshoot resulting from applying $u=\pm 1$ along the internal minimum time switching curves places the system out of the deadzone. Their omission also more clearly indicates that the optimal control is $\hat{u}=0$ in the shaded region of Figure II-6. Since this contains part of the deadzone region, control effort is unnecessary because the control objectives have been met. Since the internal minimum time switching lines, B-C and F-G, are special cases of the

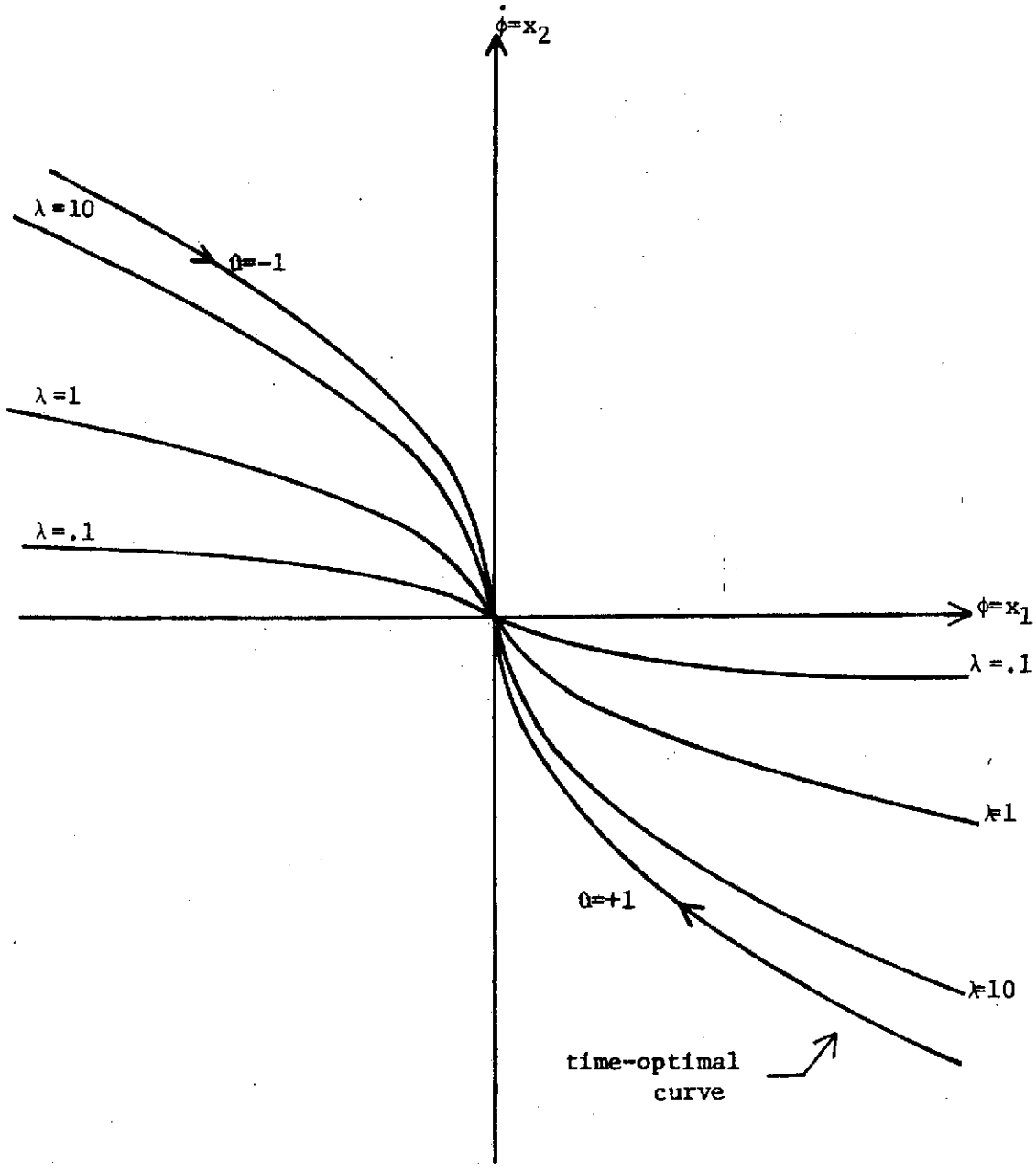

Figure II-4. Optimal weighted time-fuel switching curves for $\lambda=.1,1,10$.

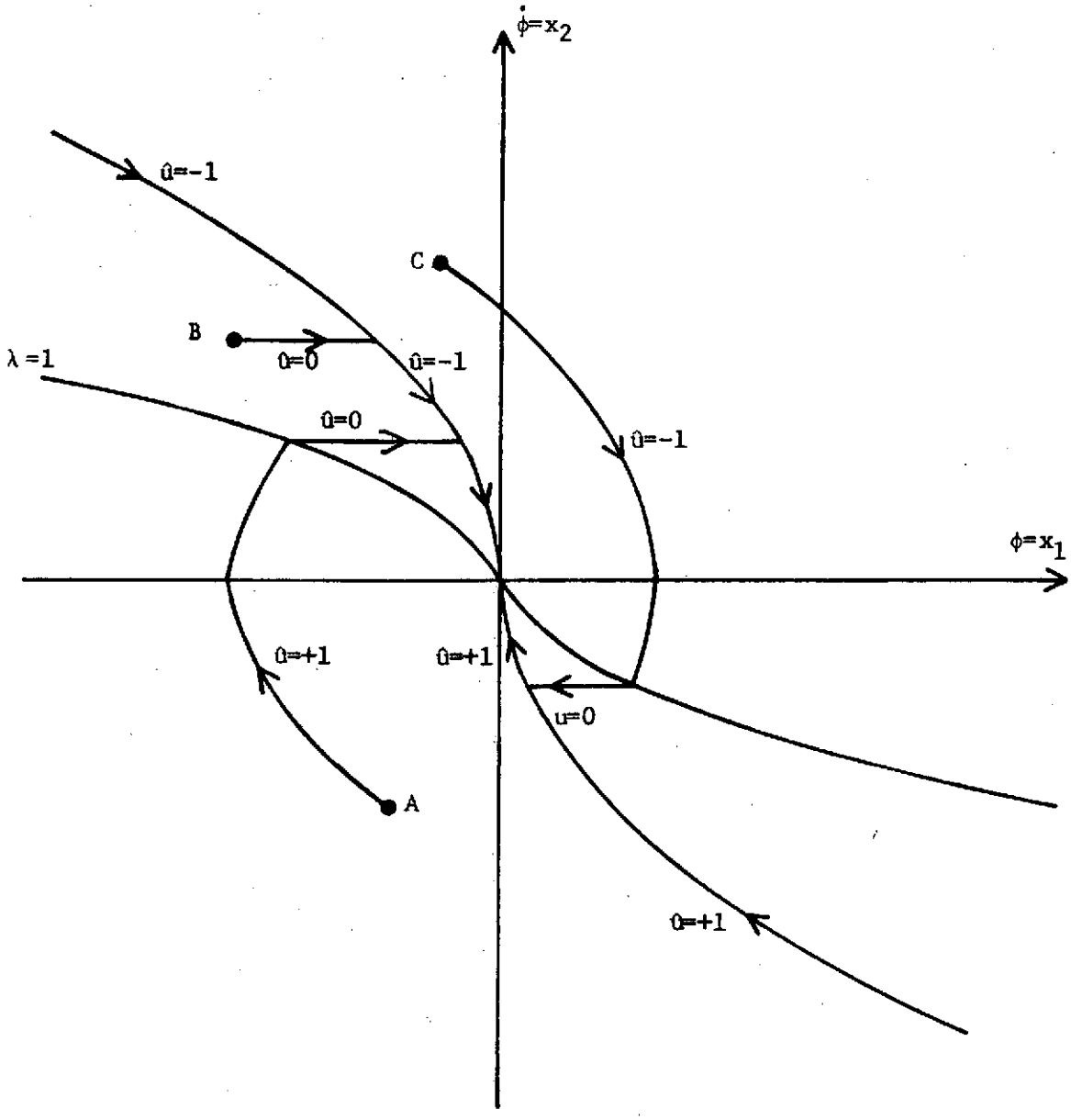

Figure II-5. Optimal weighted time-fuel trajectories for intial conditions A,B,C with $\lambda=1$.

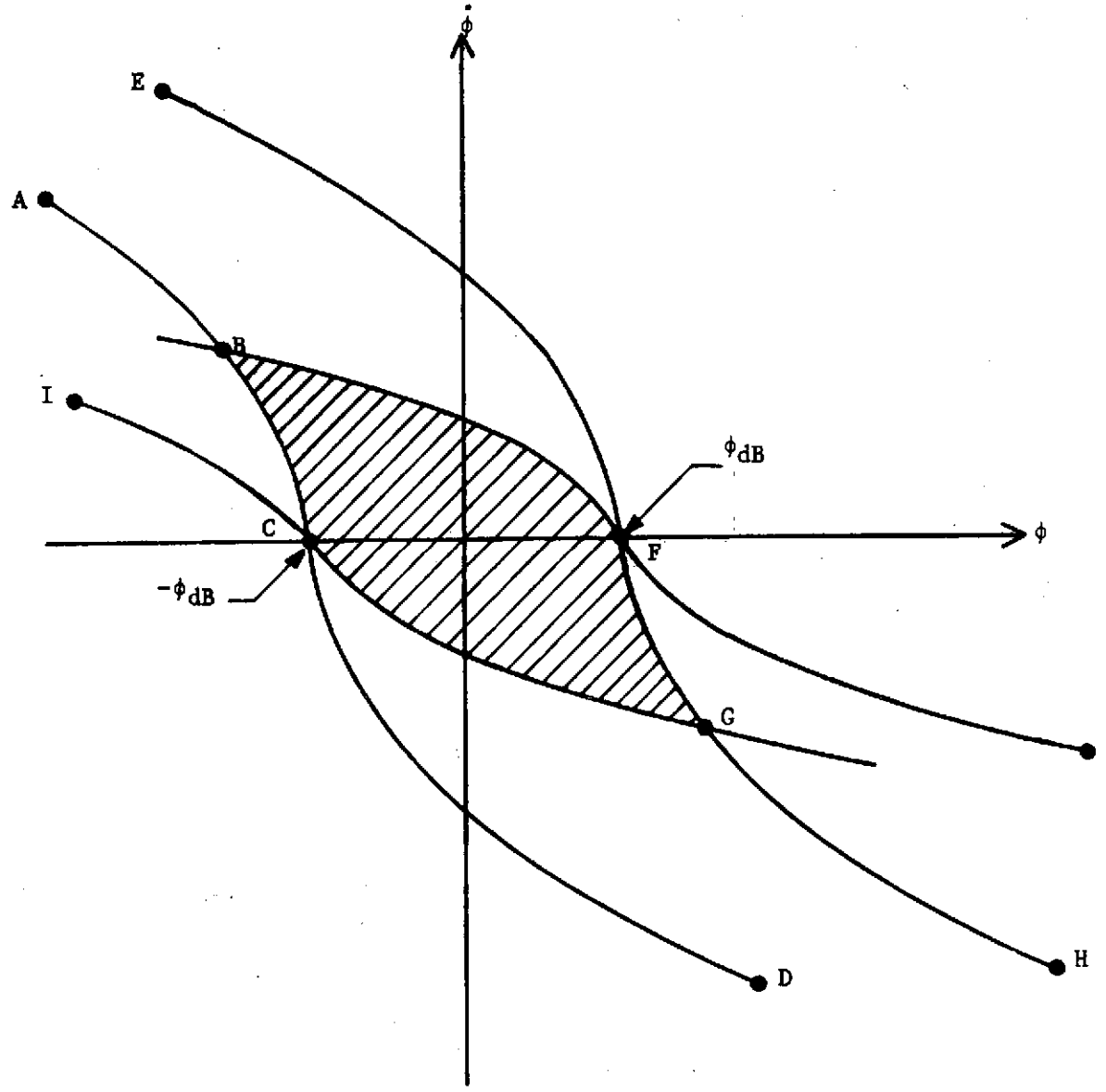

Figure II-6. Shifted weighted time-fuel optimal switching curves to give the optimal deadzone weighted time-fuel control law.

region just mentioned and $\hat{u}=0$ on both sides of these curves, they will be omitted. The resulting optimal attitude control law composed of switching curves I-C-D and E-F-J in Figure II-6 is shown in Figure II-7 along with the presently employed reaction control jet attitude control law superimposed for comparison.

The control system that gives the presently employed reaction control jet control law is shown in Figure II-8. Before determining an expression for a value of λ that gives the optimal weighted time-fuel control law that corresponds to a particular rate ledge and rate limit control law, some of the terms shown in Figures II-7 and II-8 will be defined. ϕ_R is the limiting value for ϕ in the ϕ feedback loop in Figure II-8. Figure II-7 reveals that the sloping deadzone curves reach their limiting values for $\phi=\pm\phi_R$. The maximum rate of the system in the $\hat{u}=0$ region is $\dot{\phi}_{lim}$, while the minimum rate in the $\hat{u}=0$ region for $|\phi|>\phi_R$ is $\dot{\phi}_{ledge}$. ϕ_c is the commanded vehicle attitude, and ϕ_{dB} is the width of the deadzone about ϕ_c. Finally, A_1 is the rate feedback gain.

The rate ledge and rate limit can be related to the states which, in turn, are related to λ in the phase plane. These expressions may be solved for the value of λ that gives a weighted time-fuel curve which intersects the rate ledge at $\phi=\phi_0$ as shown in Figure II-7.

For $|\phi|\leq\phi_R$ the equations for the switching curves can be determined using Figure II-8 to be

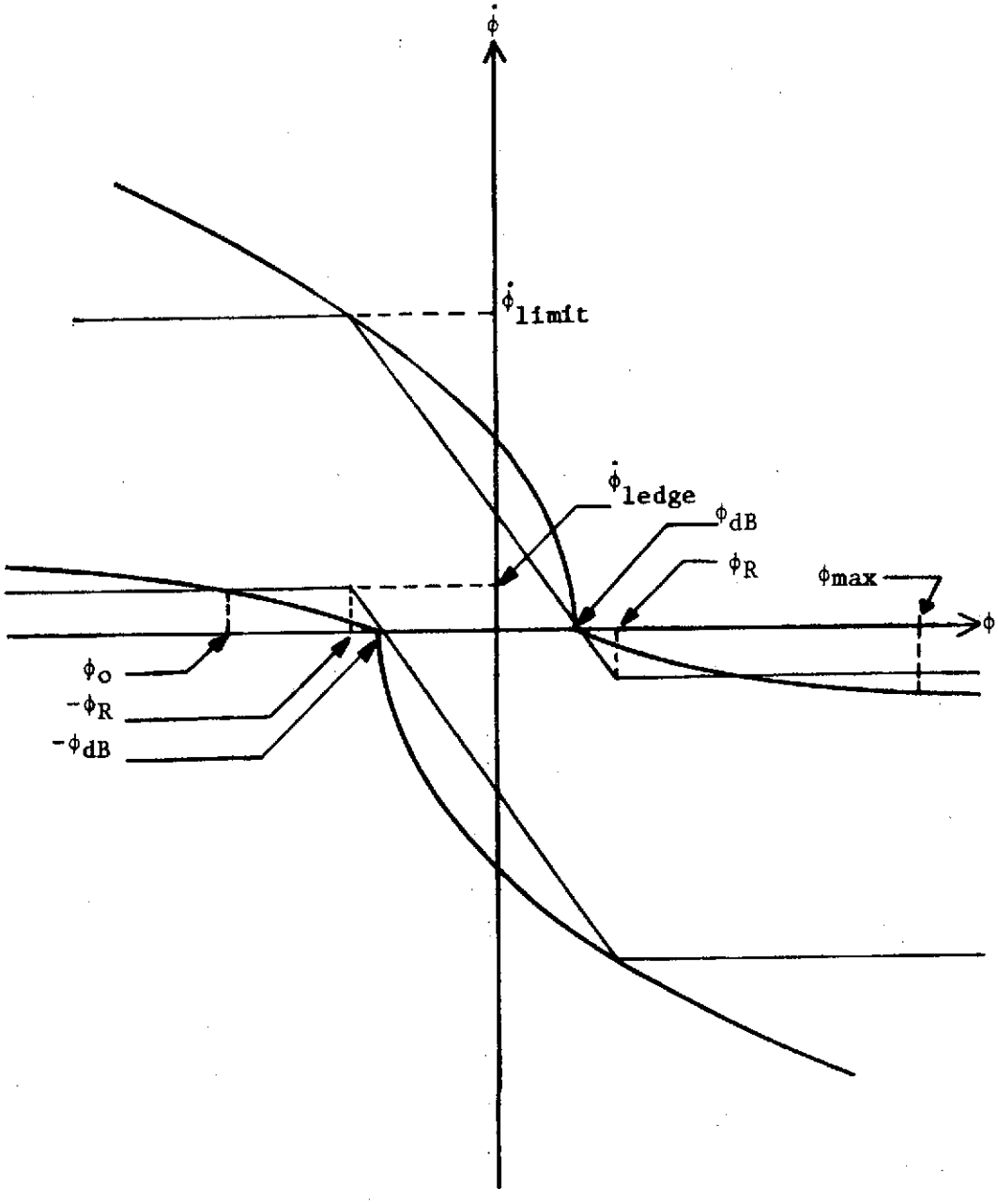

Figure II-7. Phase plane of the reaction control jet control law and the corresponding optimal control law.

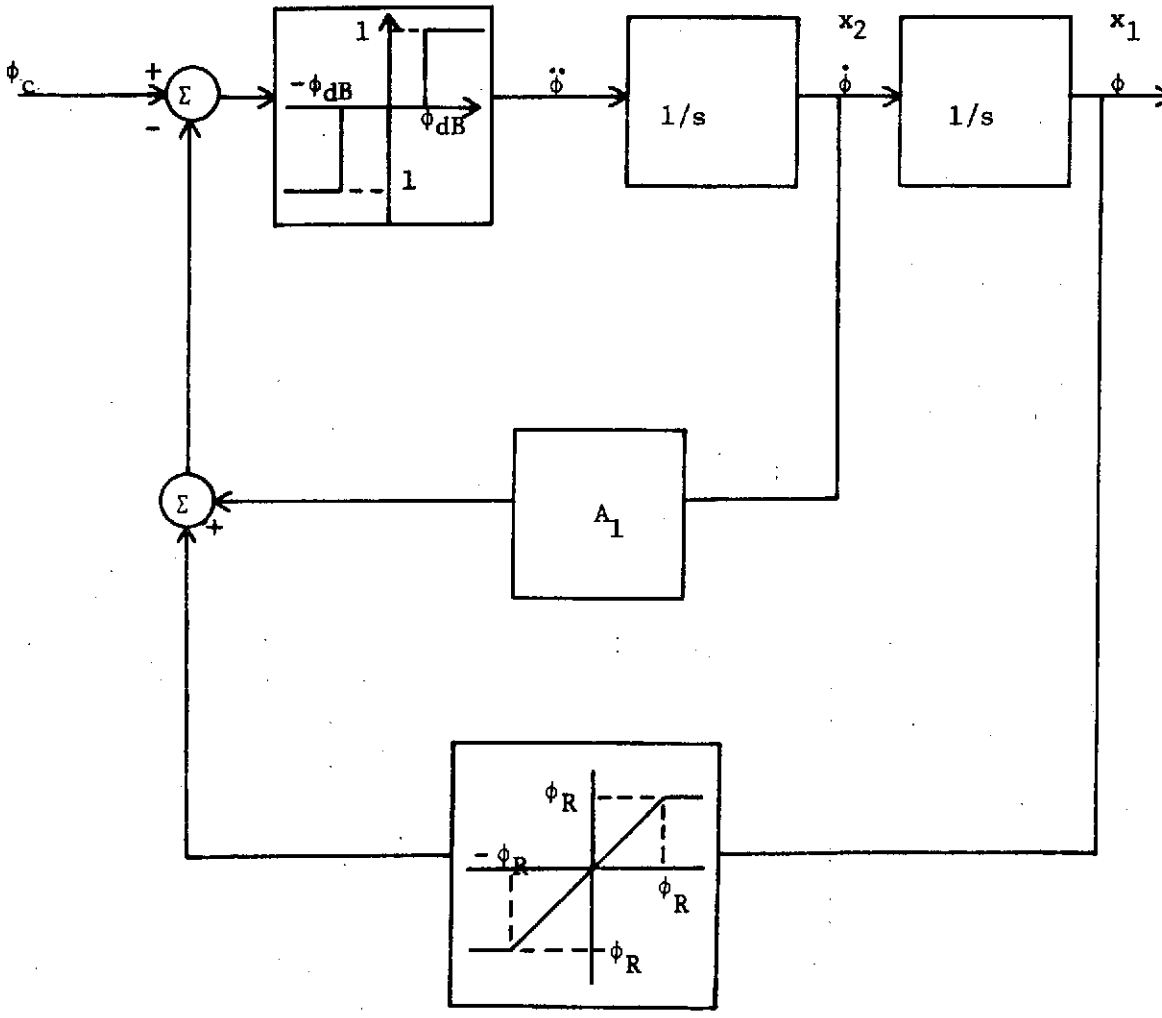

Figure II-8. Single-axis reaction control jet control system.

$$A_1\dot{\phi} + \phi = \phi_{dB}$$

$$A_1\dot{\phi} + \phi = -\phi_{dB} \qquad \text{(II-32)}$$

Equation (II-13) defines the corresponding optimal switching curves as

$$\tfrac{1}{2}\dot{\phi}^2 + \phi = \phi_{dB}$$

$$-\tfrac{1}{2}\dot{\phi}^2 + \phi = -\phi_{dB} \qquad \text{(II-33)}$$

Substituting $\pm\phi_R$ for ϕ in Equations (II-32) and (II-33), solving these equations for $\dot{\phi}$, and equating the expressions for ϕ gives the expression for A_1 to be

$$A_1 = \sqrt{\frac{\phi_R + \phi_{dB}}{2}} \qquad \text{(II-34)}$$

The rate limit and rate ledge are obtained from Equations (II-32) by solving for $\dot{\phi}$ with $\phi=\pm\phi_R$. These expressions for the rate limit and rate ledge control law are

$$\dot{\phi}_{lim} = \sqrt{2(\phi_R + \phi_{dB})} \qquad \text{(II-35)}$$

$$\dot{\phi}_{ledge} = (\phi_R - \phi_{dB})\sqrt{\frac{2}{\phi_R + \phi_{dB}}} \qquad \text{(II-36)}$$

The expression for the optimal switching curve corresponding to Equation (II-36) is given by Equation (II-30). Solving Equation (II-30) for $\dot{\phi}^2$ and including the shift from the origin to $-\phi_{dB}$ gives

$$\dot{\phi}^2 = -\frac{2\lambda}{\lambda + 4}(\phi + \phi_{dB}) \qquad \text{(II-38)}$$

Squaring Equation (II-36) and equating the expressions for $\dot{\phi}^2$ yields

$$\frac{2(\phi_R - \phi_{dB})^2}{\phi_R + \phi_{dB}} = -\frac{2\lambda}{\lambda + 4}(\phi + \phi_{dB}) \qquad \text{(II-38)}$$

Equation (II-38) may be solved for either λ or ϕ_0 corresponding to the intersection of the rate ledge and the optimal switching curve. Solving for $\phi=\phi_0$ yields

$$\phi_0 = -\frac{\lambda + 4}{\lambda}\frac{(\phi_R - \phi_{dB})^2}{\phi_R + \phi_{dB}} - \phi_{dB} \qquad \text{(II-39)}$$

while solving for λ gives

$$\lambda = \frac{-4(\phi_R - \phi_{dB})^2}{(\phi_R - \phi_{dB})^2 + (\phi + \phi_{dB})(\phi_R + \phi_{dB})} \qquad \text{(II-40)}$$

The optimal weighted time-fuel control law that most closely corresponds to a particular reaction control jet (RCJ) control system may be determined by minimizing the mean square rate errors between the two switching curves. The value of λ determined minimizes the mean square error for a given value of ϕ_{max}, the largest expected attitude error. The square error, $f(\lambda,\phi)$, is defined as

$$f(\lambda,\phi) = (\dot{\phi}_{optimal} - \dot{\phi}_{rate\ ledge})^2 \qquad \text{(II-41)}$$

Solving Equation (II-37) gives the expression for $\dot{\phi}_{optimal}$ as

$$\dot{\phi}_{optimal} = -\frac{2\lambda}{\lambda + 4}(\phi + \phi_{dB})^{1/2} \qquad \text{(II-42)}$$

$\dot{\phi}_{\text{ledge}}$ is obtained from Equations (II-32) and (II-36) as

$$\dot{\phi}_{\text{rate ledge}} = \begin{cases} -(\phi + \phi_{dB}) \left(\dfrac{2}{\phi_R + \phi_{dB}} \right)^{1/2}, & -\phi_R < \phi < -\phi_{dB} \\ (\phi_R - \phi_{dB}) \left(\dfrac{2}{\phi_R + \phi_{dB}} \right) 1/2, & -\phi_{max} < \phi < -\phi_R \end{cases} \tag{II-43}$$

The value of λ that minimizes the mean square error is obtained by solving

$$\frac{\partial}{\partial \lambda} \left[\frac{1}{\phi_{max} - \phi_{dB}} \int_{-\phi_{dB}}^{-\phi_{max}} f(\lambda, \phi) d\phi \right] = 0 \tag{II-44}$$

The integral in Equation (II-44) must be divided into two regions since $\dot{\phi}_{\text{rate ledge}}$ is defined by two different expressions over the interval from $-\phi_{dB}$ to $-\phi_{max}$. Substituting Equations (II-42) and (II-43) into Equation (II-41) and performing the squaring operation yields

$$f(\lambda, \phi) = \begin{cases} f_1(\lambda, \phi) & , \quad -\phi_R < \phi < -\phi_{dB} \\ f_2(\lambda, \phi) & , \quad -\phi_{max} < \phi < -\phi_R \end{cases} \tag{II-45}$$

where, $$f_1(\lambda, \phi) = -\frac{2\lambda(\phi + \phi_{dB})}{\lambda + 4} + 4(\phi + \phi_{dB}) \left(\frac{-\lambda[\phi + \phi_{dB}]}{(\lambda + 4)(\phi_R + \phi_{dB})} \right)^{1/2} +$$

$$\frac{2(\phi + \phi_{dB})^2}{\phi_R + \phi_{dB}} \tag{II-46}$$

and $$f_2(\lambda,\phi) = -\frac{2\lambda(\phi+\phi_{dB})}{\lambda+4} - 4(\phi_R-\phi_{dB})\left(\frac{\lambda(\phi+\phi_{dB})}{(\lambda+4)(\phi_R+\phi_{dB})}\right)^{1/2} + \frac{2(\phi_R-\phi_{dB})^2}{\phi_R+\phi_{dB}} \qquad \text{(II-47)}$$

Using (II-45), Equation (II-44) now becomes

$$\frac{\partial}{\partial\lambda}\left[\int_{-\phi_{dB}}^{-\phi_R} f_1(\lambda,\phi)\,d\phi + \int_{-\phi_R}^{-\phi_{max}} f_2(\lambda,\phi)\,d\phi\right] = 0 \qquad \text{(II-48)}$$

where Equation (II-44) has been multiplied by the constant $(\phi_{max} - \phi_{dB})$.

Evaluation of equations in the form of Equation (II-44) is aided with the use of Leibniz rule, which is

$$\frac{\partial}{\partial t}\int_{a(t)}^{b(t)} g(t,u)\,du = \int_{a(t)}^{b(t)} \frac{\partial g(t,u)}{\partial t}\,du + g(t,a(t))\frac{db(t)}{dt} - g(t,b(t))\,\frac{da(t)}{dt} \qquad \text{(II-49)}$$

Applying Leibniz rule, Equation (II-48) becomes

$$\int_{-\phi_{dB}}^{-\phi_R} \frac{\partial f_1(\lambda,\phi)}{\partial\lambda}\,d\phi + \int_{-\phi_R}^{-\phi_{max}} \frac{\partial f_2(\lambda,\phi)}{\partial\lambda}\,d\phi = 0 \qquad \text{(II-50)}$$

The partial derivatives required in Equation (II-50) are obtained by taking the partial derivatives with respect to λ of Equations (II-46) and (II-47). These partial derivatives are

$$\frac{\partial f_1(\lambda,\phi)}{\partial\lambda} = -\frac{8(\phi+\phi_{dB})}{(\lambda+4)^2} + \frac{8\left[-(\phi+\phi_{dB})\right]^{3/2}}{\left[\lambda(\phi_R+\phi_{dB})\right]^{1/2}(\lambda+4)^{3/2}}$$

$$\frac{\partial f_2(\lambda,\phi)}{\partial\lambda} = -\frac{8(\phi+\phi_{dB})}{(\lambda+4)^2} - \frac{8(\phi_R-\phi_{dB})\left[-(\phi+\phi_{dB})\right]^{1/2}}{\left[\lambda(\phi_R+\phi_{dB})\right]^{1/2}(\lambda+4)^{3/2}} \qquad \text{(II-51)}$$

Substituting Equations (II-51) into Equation (II-50) and evaluating the indicated integrals yields

$$\frac{K_1}{\lambda^{1/2}(\lambda+4)^{3/2}} - \frac{K_2}{(\lambda+4)^2} + \frac{K_3}{\lambda^{1/2}(\lambda+4)^{3/2}} = 0 \qquad \text{(II-52)}$$

where $$K_1 = \frac{8\left[(2/5)(\phi_R-\phi_{dB})^{5/2}\right]}{(\phi_R+\phi_{dB})^{1/2}} \qquad \text{(II-53a)}$$

$$K_2 = 4(\phi_{max}-\phi_{dB})^2 \qquad \text{(II-53b)}$$

$$K_3 = \frac{8\left[(2/3)(\phi_R-\phi_{dB})\right]}{(\phi_R+\phi_{dB})^{1/2}}\left[(\phi_{max}-\phi_{dB})^{3/2} - (\phi_R-\phi_{dB})^{5/2}\right] \qquad \text{(II-53c)}$$

Combining like terms in Equations (II-53a) and (II-53c), then substituting the result in Equation (II-52) gives

$$\frac{K_4}{\lambda^{1/2}(\lambda+4)^{3/2}} + \frac{K_2}{(\lambda+4)^2} = 0 \qquad \text{(II-54)}$$

where $$K_4 = \frac{(16/3)(\phi_R-\phi_{dB})(\phi_{max}-\phi_{dB})^{3/2} - (32/15)(\phi_R-\phi_{dB})^{5/2}}{(\phi_R+\phi_{dB})^{1/2}} \qquad \text{(II-55)}$$

Multiplying Equation (II-54) by $\lambda(\lambda + 4)^2$ and transposing terms so that only terms involving λ are on one side of the equation yields,

$$\left(\frac{\lambda}{\lambda + 4}\right)^{1/2} = \frac{K_4}{K_2} \qquad \text{(II-56)}$$

Squaring Equation (II-56) and solving for λ gives the expression for the λ that minimizes the mean square rate error between the two switching curves as

$$\lambda = \frac{4K_4^2}{K_2^2 - K_4^2} \qquad \text{(II-57)}$$

As an example, suppose a RCJ control system has $\phi_{dB} = 2$, $\phi_R = 4$, and $\phi_{max} = 10$. Figure II-7 shows the relationship of these terms to the control law. To find the weighted time-fuel optimal control most closely corresponding to the RCJ system, the constants K_2 and K_4 are first computed using Equations (II-53) and (II-55), respectively. For the example, these constants are calculated to be

$$K_2 = 256$$

$$K_4 = 93$$

Substituting these values into Equation (II-57) yields λ as

$$\lambda = .61$$

This system places more emphasis on conserving fuel since the control law penalizes fuel consumption 1.7 times as heavily as it does time.

However, since fuel is limited to the fixed amount the vehicle can carry, a RCJ system will usually place more emphasis on fuel conservation.

The previous results were obtained from the standpoint of beginning with the conventional RCJ control system with the parameters ϕ_{dB}, ϕ_R, and ϕ_{max} given. The optimal weighted time-fuel control system that most closely corresponds to the RCJ control system is obtained by solving Equation (II-57) for the λ that minimizes the mean square error between the two rate ledge switching curves. Now the problem will be approached in the reverse direction. The value of λ in the weighted time-fuel performance measure along with the desired ϕ_{dB} and ϕ_{max} for the RCJ control system are given. The problem is to find the RCJ system most closely corresponding to this optimal control system.

An expression for ϕ_R can be obtained in a manner analogous to the technique used to obtain an expression for λ. For this case, Equation (II-44) becomes

$$\frac{\partial}{\partial \phi_R}\left[\frac{1}{\phi_{max} - \phi_{dB}} \int_{-\phi_{dB}}^{-\phi_{max}} f(\phi_R, \phi)\, d\phi\right] \qquad \text{(II-58)}$$

where $f(\phi_R, \phi)$ is the same expression as that defined for $f(\lambda, \phi)$ in Equation (II-41) with the roles of λ and ϕ_R as known and unknown variables interchanged. Applying the same procedure employed to determine an expression for λ results in a sixth order expression in ϕ_R. This expression can be solved with a digital computer using root-solving algorithms. However, a more appealing approach is presented here.

The initial step is to obtain a second order expression in ϕ_R in terms of ϕ_0 using Equation (II-39). Rearranging Equation (II-39) and performing the squaring operation on $(\phi_R - \phi_{dB})$ yields

$$\phi_R^2 + a_1\phi_R + a_0 = 0 \tag{II-59}$$

where $$a_1 = -2\phi_{dB} + \frac{\lambda}{\lambda + 4}(\phi_0 + \phi_{dB})$$

$$a_0 = \phi_{dB}^2 + \frac{\lambda}{\lambda + 4}(\phi_0 + \phi_{dB})\phi_{dB}$$

The quadratic formula is used to determine ϕ_R for a given ϕ_0 as

$$\phi_R = \frac{-a_1 \pm (a_1^2 - 4a_0)^{1/2}}{2} \tag{II-60}$$

Equation (II-60) is used to obtain an initial guess of the value of ϕ_R. This value of ϕ_R is obtained by initially guessing the value of ϕ_0 to be midway between ϕ_{dB} and ϕ_{max} since this would be a reasonable guess for the value that minimizes the mean square error. Therefore,

$$\phi_0 = -\phi_{dB} - \frac{\phi_{max} - \phi_{dB}}{2} \tag{II-61}$$

for the initial guess of ϕ_0.

In the expression for λ given by Equation (II-57), only K_4 is a function of ϕ_R. For the given value of λ, the desired value of K_4, K_{4d}, is obtained by solving (II-56) to give

$$K_{4d} = K_2\left(\frac{\lambda}{\lambda + 4}\right)^{1/2} \tag{II-62}$$

A Taylor series expansion of $K_4(\phi_R)$ is obtained from Equation (II-55) in order to systematically improve the initial guess at ϕ_R. Using only the linear terms in the Taylor series, Equation (II-55) becomes

$$K_4(\phi_R) = K_4(\phi_{RO}) + K_4'(\phi_{RO})\ \delta\phi_R \tag{II-63}$$

where $\delta\phi_R = \phi_R - \phi_{RO}$

$$K_4'(\phi_{RO}) = (16/3)(\phi_{max} - \phi_{dB})^{3/2}B - (32/15)(C - D) \tag{II-64a}$$

$$B = \frac{(\phi_{RO} + \phi_{dB})^{1/2} - .5(\phi_R + \phi_{dB})^{-1/2}(\phi_{RO} - \phi_{dB})}{(\phi_{RO} + \phi_{dB})} \tag{II-64b}$$

$$C = \frac{2.5(\phi_{RO} - \phi_{dB})^{3/2}(\phi_{RO} + \phi_{dB})^{1/2}}{(\phi_{RO} + \phi_{dB})} \tag{II-64c}$$

$$D = \frac{.5(\phi_{RO} + \phi_{dB})^{-1/2}(\phi_{RO} - \phi_{dB})^{5/2}}{(\phi_{RO} + \phi_{dB})} \tag{II-64d}$$

ϕ_{RO} is the present guess for ϕ_R and $K_4(\phi_{RO})$ is given by Equation (II-55). Solving (II-63) for $\delta\phi_R$ used to update ϕ_R yields

$$\delta\phi_R = \frac{K_4(\phi_R) - K_4(\phi_{RO})}{K_4'(\phi_{RO})} = \frac{K_{4d} - K_4(\phi_{RO})}{K_4'(\phi_{RO})} \tag{II-65}$$

The improved guess for ϕ_R is now given as

$$\phi_R = \phi_{R0} + \delta\phi_R \qquad \text{(II-66)}$$

As an example of applying this procedure, consider the earlier example where λ was computed to be .61 with $\phi_{dB} = 2$ and $\phi_{max} = 10$. The initial value of ϕ_0 is computed from (II-61) as

$$\phi_0 = -6$$

Using this value of ϕ_0, ϕ_R is determined from (II-60) to be

$$\phi_R = 3.74$$

$K_4(\phi_{R0})$ is computed from (II-55) as

$$K_4(3.74) = 83.5$$

K_{4d} is determined from (II-62) to be

$$K_{4d} = 93$$

Next, solving (II-65) for the update, $\delta\phi_R$, gives

$$\delta\phi_R = \frac{93 - 83.5}{37.8} = .252$$

The new value of ϕ_R is given by (II-66) as

$$\phi_R = 3.74 + .252 = 3.992$$

Computing the new value of $K_4(\phi_{R0})$ gives

$$K_4(3.99) = 92.9$$

For this case only one update was required to obtain an accurate value for ϕ_R. This value of ϕ_R can then be used to determine A_1 using Equation (II-34), the rate limit using Equation (II-35), and the rate ledge using Equation (II-36). These values are computed to be

$$A_1 = 1.73$$

$$\dot{\phi}_{lim} = 3.46$$

$$\dot{\phi}_{ledge} = 1.16$$

These values along with the given ϕ_{dB} determine the RCJ control system that most closely corresponds to the given optimal weighted time-fuel control system. The results obtained in these examples illustrate the uniqueness of these procedures. That is, if the procedure is applied to find an optimal weighted time-fuel control system corresponding to a given RCJ system and then the reverse procedure applied to this optimal time-fuel system, the RCJ system obtained will be the original one. Figure II-9 shows the optimal control system and its corresponding RCJ control system for the two examples given.

In summary, under the assumption of second order dynamics, the conventional RCJ control system is shown to be a good linear approximation to an optimal weighted time-fuel control system. Furthermore, for ϕ_{dB}, ϕ_{max}, and ϕ_R given, an expression is derived that gives the value of λ weighting time and fuel. This λ is chosen such that the mean square error between the switching curves of the RCJ system and the optimal control system corresponding to this value of λ is minimized.

Also, an iterative procedure is presented to determine ϕ_R for the RCJ control system that corresponds to an optimal weighted time-fuel control system with λ given. This procedure also requires knowledge of the desired ϕ_{dB} and ϕ_{max} for the RCJ control system. The procedure produces unique results in that applying the procedure followed by its reverse procedure yields the original system.

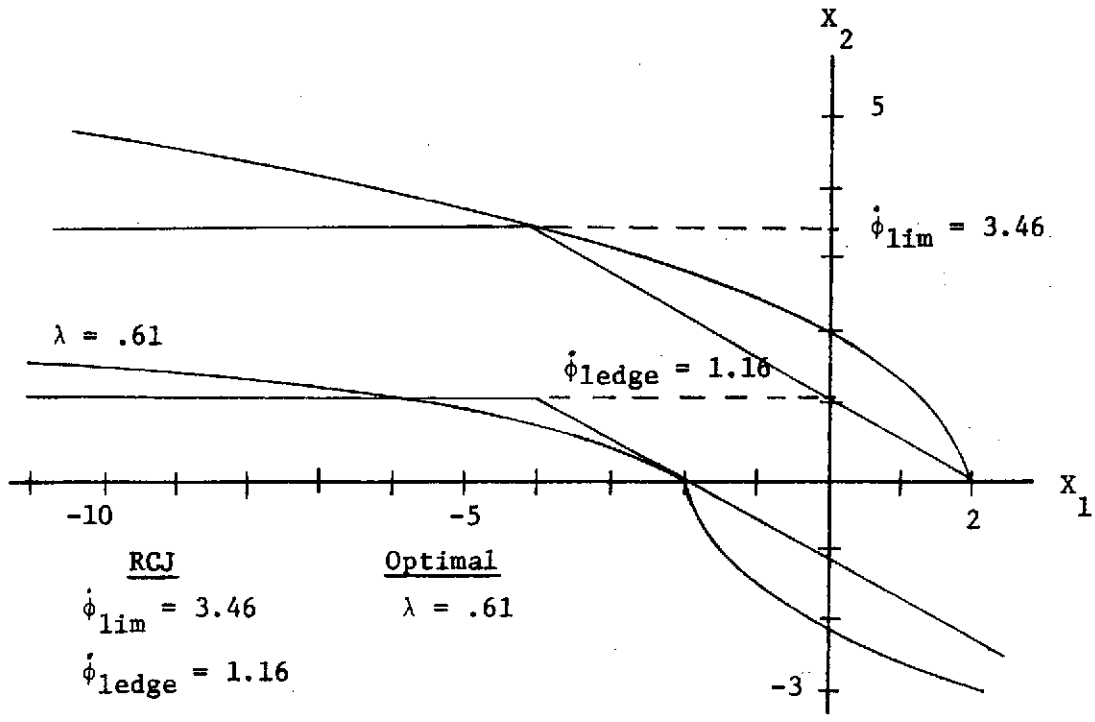

Figure II-9. Phase Plane for Example System.

III. SOME BASIC IDEAS RELATED TO THE USE OF CONTROL MOMENT GYROS FOR ATTITUDE CONTROL

A reaction control jet (RCJ) mass expulsion system can provide control within a band of a desired operating state. Control moment gyros (CMGs), based on the principle of momentum exchange, can provide the fine-pointing capability required for many space missions. Morine and O'Connor describe the CMG and its relative merits in [2].

The principle of momentum exchange is a consequence of Newton's second law of angular motion which states that the total external moment, $\vec{M}_{ext}$, acting on a system, is proportional to the time rate of change of angular momentum with respect to inertial space. This can be written as

$$\vec{M}_{ext} = \left\{ \frac{d\vec{H}_{system}}{dt} \right\}_{\text{Inertial Space}} \qquad \text{(III-1)}$$

Considering the system to be composed of a vehicle and a controller, Equation (III-1) can be integrated to yield

$$\int \vec{M}_{ext} dt = \vec{H}_{ext} = \vec{H}_{control} + \vec{H}_{vehicle} - \vec{H}_{system}(0+) \qquad \text{(III-2)}$$

Equation (III-2) illustrates that the controller momentum can be used to balance external torques as well as change the spacecraft attitude by varying the vehicle angular momentum.

Since electrical energy is used as the prime source of power, the concept of momentum exchange using CMGs is desirable because it provides continuous vehicle control and a recoverable energy source. Cyclic disturbance torques can also be handled on a continuous basis over a long period of time. However, constant external disturbances applied to the vehicle will eventually cause the controller to reach its maximum capacity, and thus saturate the CMG. This saturation will require the expulsion of propellants to remove some momentum from the saturated CMG. This propellant expulsion task may be accomplished at a convenient time during the mission.

The CMG is essentially a gimballed wheel rotating at a constant speed which provides a constant angular momentum magnitude capable of variable orientation relative to the spacecraft. Exchange of momentum between the vehicle and the controller is effected by causing a change in direction of the constant momentum magnitude of the CMG.

Figure III-1 shows schematically a two degree of freedom CMG. It consists of a wheel that rotates at a constant speed. This wheel is held in a housing which is called the inner gimbal. The inner gimbal is coupled to the outer gimbal through the (1) pivot which is perpendicular to the wheel spin vector as shown in Figure III-1. The outer gimbal is held to the base through the (3) pivot which is perpendicular to the (1) pivot. The (1) and (3) pivots are driven by geared D. C. torque motors.

CMGs offer several advantages over other momentum exchange devices such as reaction wheels. Since the CMG operates at a constant

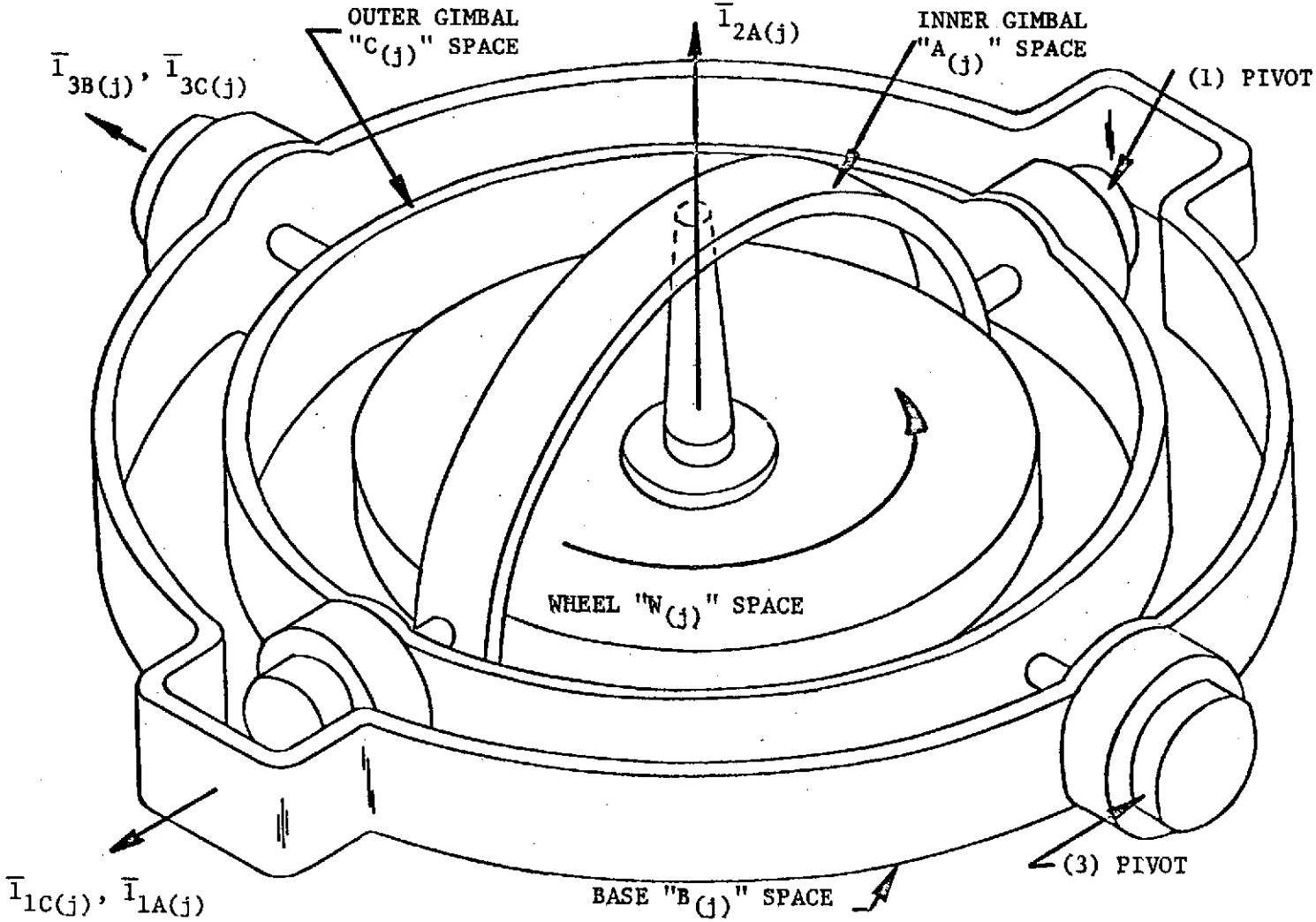

Figure III-1. The "j" control moment gyro schematic.

speed for which the efficiency can be optimized, its efficiency is greatly improved for most operating momentum values. Larger maximum moment control can be obtained will relatively small turning rates of the large constant momentum. Another CMG advantage is better bandwidth over the reaction wheel which has a limited bandwidth due to the physical characteristics of the wheel. A final advantage of the CMG is that it has a more linear approach to saturation than do reaction wheels. These advantages coupled with the fact that the CMG provides continuous control and a recoverable energy source makes the CMG an attractive device for long duration fine-pointing attitude control missions.

A. CMG Equations of Motion

For any control system using CMGs, it is first necessary to know the relationship between the reaction torque of the CMG configuration and the gimbal angles and gimbal rates of the gyros. Throughout this analysis, the CMG configuration assumed will be the conventional SIXPAC configuration as shown in Figure III-2.

The relationship between the gyro gimbal angles and the reaction torque will be obtained by first arriving at an expression for the angular momentum of the configuration, and then applying Equation (III-1) to determine the torque.

The initial step in determining an expression for the angular momentum is to define three gyro spaces [2]. Referring again to Figure III-1, the "$A_{(j)}$" space or inner gimbal is described by the coordinate system $\overline{1}_{1A(j)}$, $\overline{1}_{2A(j)}$, and $\overline{1}_{3A(j)}$. The "$A_{(j)}$ space coordinate system

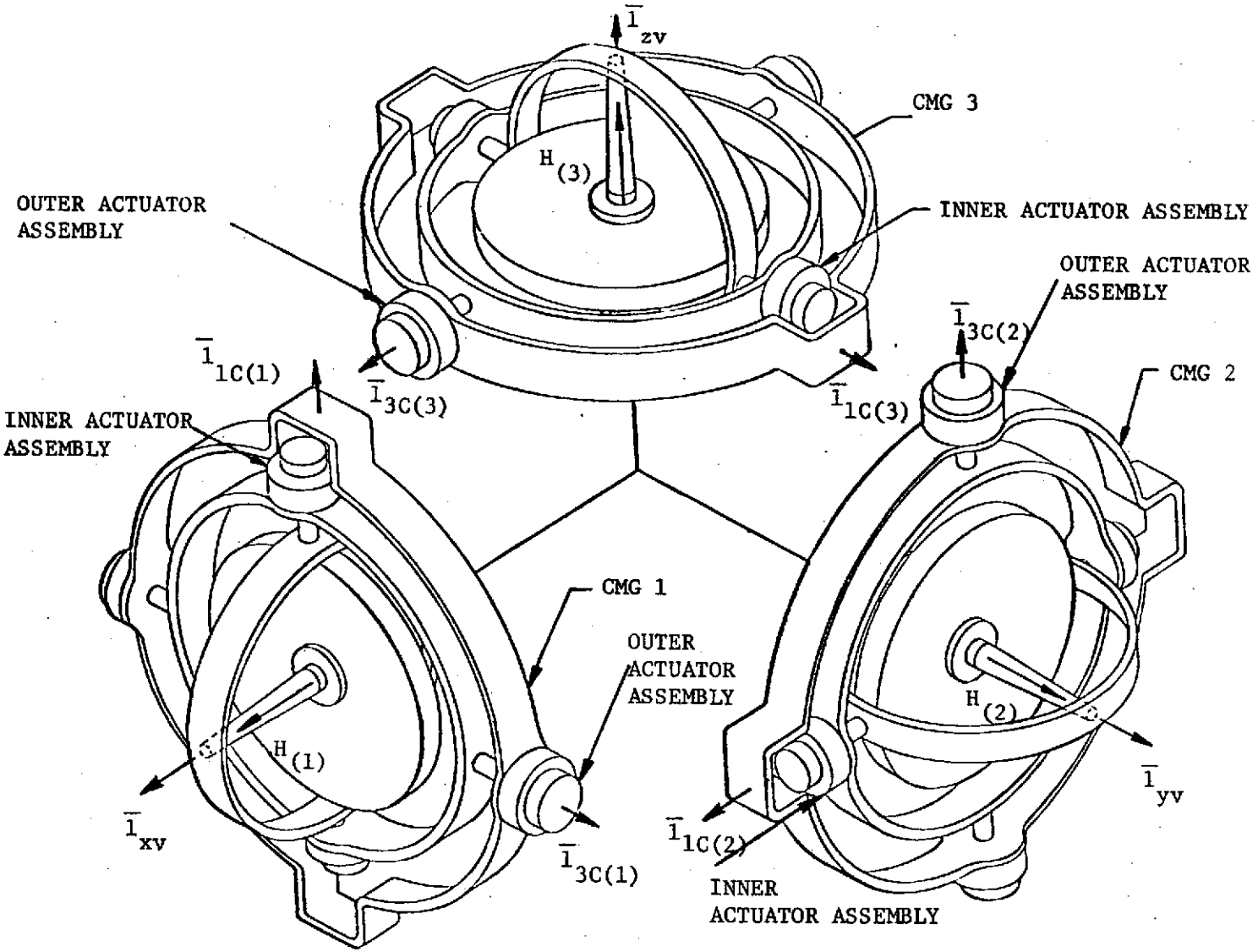

Figure III-2. The Conventional CMG SIXPAC configuration

is defined such that the $\bar{1}_{2A(j)}$ vector is along the spin reference axis, the $\bar{1}_{1A(j)}$ vector is along the (1) or inner pivot, and the $\bar{1}_{3A(j)}$ vector completes the orthogonal coordinate system. The "$C_{(j)}$" space or outer gimbal space is described by the coordinate system $\bar{1}_{1C(j)}$, $\bar{1}_{2C(j)}$, and $\bar{1}_{3C(j)}$ which is defined such that the $\bar{1}_{1A(j)}$ and $\bar{1}_{1C(j)}$ vectors are coincident, the $\bar{1}_{3C(j)}$ vector lies along the (3) or outer pivot, and the $\bar{1}_{2C(j)}$ vector completes the orthogonal coordinate system. The base of the CMG or "$B_{(j)}$" space is described by the $\bar{1}_{1B(j)}$, $\bar{1}_{2B(j)}$, and $\bar{1}_{3B(j)}$ coordinate system. With these spaces defined, the zero position of the CMG is defined when the vectors $\bar{1}_{1A(j)}$, $\bar{1}_{2A(j)}$, and $\bar{1}_{3A(j)}$ are coincident with the vectors $\bar{1}_{1C(j)}$, $\bar{1}_{2C(j)}$, and $\bar{1}_{3C(j)}$ and coincident with the vectors $\bar{1}_{1B(j)}$, $\bar{1}_{2B(j)}$, and $\bar{1}_{3B(j)}$.

The (1) pivot angle $\delta_{1(j)}$ is defined positively when the inner gimbal is rotated in a positive direction about the $\bar{1}_{1A(j)}$ vector with respect to the outer gimbal as shown in Figure III-3. Similarly, the (3) pivot angle $\delta_{3(j)}$ is positive when the outer gimbal is rotated in a positive direction about the $\bar{1}_{3C(j)}$ vector with respect to the base as shown in Figure III-4.

Using the definitions of the coordinate systems and gimbal angles, the transformation matrices from "$A_{(j)}$" to "$B_{(j)}$" space, "$A_{(j)}$" to "$C_{(j)}$" space, and "$C_{(j)}$" to "$B_{(j)}$" space can be obtained. These transformation matrices are

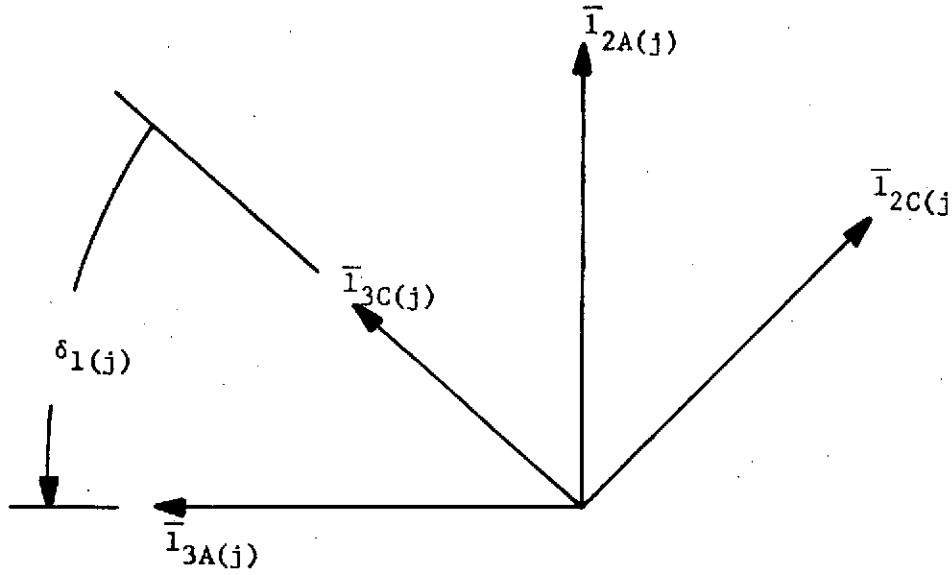

Figure III-3. Definition of the (1) pivot angle $\delta_{1(j)}$.

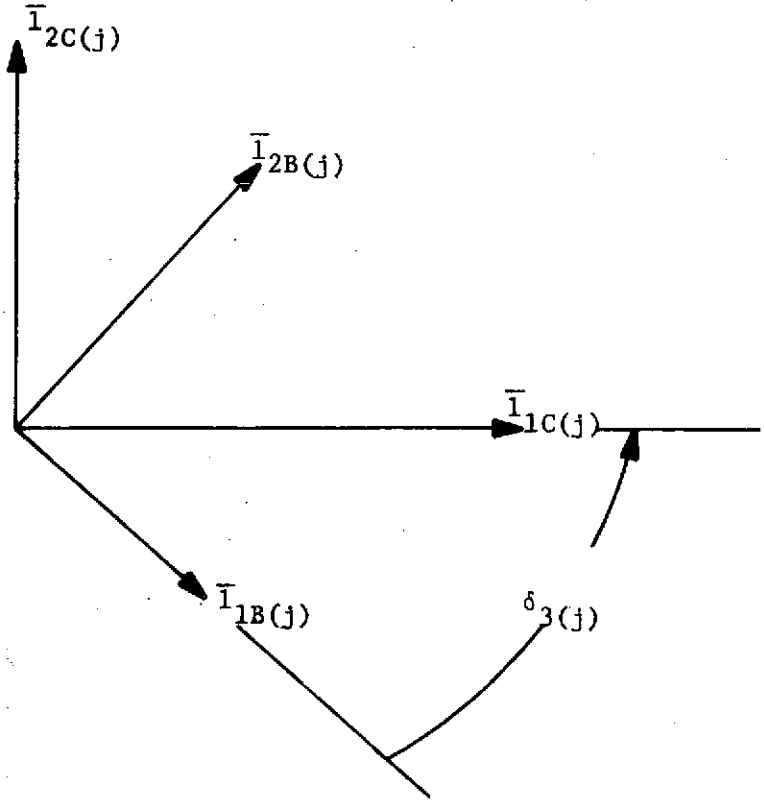

Figure III-4. Definition of the (3) pivot angle $\delta_{3(j)}$.

$$\begin{bmatrix} H_{1C(j)} \\ H_{2C(j)} \\ H_{3C(j)} \end{bmatrix} = \begin{bmatrix} 1 & 0 & 0 \\ 0 & C\delta_{1(j)} & -S\delta_{1(j)} \\ 0 & S\delta_{1(j)} & C\delta_{1(j)} \end{bmatrix} \begin{bmatrix} H_{1A(j)} \\ H_{2A(j)} \\ H_{3A(j)} \end{bmatrix} \qquad \text{(III-3)}$$

$$\begin{bmatrix} H_{1B(j)} \\ H_{2B(j)} \\ H_{3B(j)} \end{bmatrix} = \begin{bmatrix} C\delta_{3(j)} & -S\delta_{3(j)} & 0 \\ S\delta_{3(j)} & C\delta_{3(j)} & 0 \\ 0 & 0 & 1 \end{bmatrix} \begin{bmatrix} H_{1C(j)} \\ H_{2C(j)} \\ H_{3C(j)} \end{bmatrix} \qquad \text{(III-4)}$$

$$\begin{bmatrix} H_{1B(j)} \\ H_{2B(j)} \\ H_{3B(j)} \end{bmatrix} = \begin{bmatrix} C\delta_{3(j)} & -S\delta_{3(j)}C\delta_{1(j)} & S\delta_{3(j)}S\delta_{1(j)} \\ S\delta_{3(j)} & C\delta_{3(j)}C\delta_{1(j)} & -C\delta_{3(j)}S\delta_{1(j)} \\ 0 & S\delta_{1(j)} & C\delta_{1(j)} \end{bmatrix} \begin{bmatrix} H_{1A(j)} \\ H_{2A(j)} \\ H_{3A(j)} \end{bmatrix} \qquad \text{(III-5)}$$

where $S\delta_{i(j)} = \sin\delta_{i(j)}$ $\quad i = 1,3;\ j = 1,2,3$

and $C\delta_{i(j)} = \cos\delta_{i(j)}$ $\quad i = 1,3;\ j = 1,2,3$

This designation for sines and cosines of angles will be employed throughout this analysis.

Referring to Figure III-2, the transformation matrices from the base coordinate system of each of the CMGs to the vehicle coordinate system are determined for the (1) CMG to be

$$\begin{bmatrix} \bar{l}_{xv} \\ \bar{l}_{yv} \\ \bar{l}_{zv} \end{bmatrix} = \begin{bmatrix} 0 & 1 & 0 \\ 0 & 0 & 1 \\ 1 & 0 & 0 \end{bmatrix} \begin{bmatrix} \bar{l}_{1B(1)} \\ \bar{l}_{2B(1)} \\ \bar{l}_{3B(1)} \end{bmatrix} \qquad \text{(III-6)}$$

and for the (2) CMG to be

$$\begin{bmatrix} \bar{l}_{xv} \\ \bar{l}_{yv} \\ \bar{l}_{zv} \end{bmatrix} = \begin{bmatrix} 1 & 0 & 0 \\ 0 & 1 & 0 \\ 0 & 0 & 1 \end{bmatrix} \begin{bmatrix} \bar{l}_{1B(2)} \\ \bar{l}_{2B(2)} \\ \bar{l}_{3B(2)} \end{bmatrix} \qquad \text{(III-7)}$$

and for the (3) CMG to be

$$\begin{bmatrix} \bar{l}_{xv} \\ \bar{l}_{yv} \\ \bar{l}_{zv} \end{bmatrix} = \begin{bmatrix} 0 & 0 & 1 \\ 1 & 0 & 0 \\ 0 & 1 & 0 \end{bmatrix} \begin{bmatrix} \bar{l}_{1B(3)} \\ \bar{l}_{2B(3)} \\ \bar{l}_{3B(3)} \end{bmatrix} \qquad \text{(III-8)}$$

Equations (III-6), (III-7), and (III-8) can be used to determine the resultant momentum vector of the CMG cluster in vehicle coordinates as

$$\begin{bmatrix} H_{xv} \\ H_{yv} \\ H_{zv} \end{bmatrix} = \begin{bmatrix} H_{2B(1)} + H_{1B(2)} + H_{3B(3)} \\ H_{3B(1)} + H_{2B(2)} + H_{1B(3)} \\ H_{1B(1)} + H_{3B(2)} + H_{2B(3)} \end{bmatrix} \qquad \text{(III-9)}$$

Now, since the vector $\bar{l}_{2A(j)}$ in "$A_{(j)}$" space is defined to be along the spin reference axis, the transformation from "$A_{(j)}$" space to "$B_{(j)}$" space can be used to obtain the resultant momentum vector of the CMG configuration in terms of the momentum magnitude of each CMG. Assuming the momentum for each CMG to be H_0, the momentum vector for the jth CMG can be written in "$A_{(j)}$" space as

$$\vec{H}_{(j)} = \begin{bmatrix} 0 \\ H_0 \\ 0 \end{bmatrix} = \begin{bmatrix} H_{1A(j)} \\ H_{2A(j)} \\ H_{3A(j)} \end{bmatrix} \tag{III-10}$$

Substituting Equation (III-10) into Equation (III-5) gives the momentum vector of the jth CMG in "$B_{(j)}$" space as

$$\vec{H}_{(j)} = \begin{bmatrix} -S\delta_{3(j)}C\delta_{1(j)} \\ C\delta_{3(j)}C\delta_{1(j)} \\ S\delta_{1(j)} \end{bmatrix} H_0 = \begin{bmatrix} H_{1B(j)} \\ H_{2B(j)} \\ H_{3B(j)} \end{bmatrix} \tag{III-11}$$

Substituting the expressions for the CMG momentums in "$B_{(j)}$" space from Equation (III-11) into Equation (III-9) yields the expression for the momentum of the CMG cluster in vehicle coordinates as

$$\begin{bmatrix} H_{xv} \\ H_{yv} \\ H_{zv} \end{bmatrix} = \begin{bmatrix} C\delta_{3(1)}C\delta_{1(1)} & -S\delta_{3(2)}C\delta_{1(2)} & + S\delta_{1(3)} \\ S\delta_{1(1)} & + C\delta_{3(2)}C\delta_{1(2)} & -S\delta_{3(3)}C\delta_{1(3)} \\ -S\delta_{3(1)}C\delta_{1(1)} & + S\delta_{1(2)} & + C\delta_{3(3)}C\delta_{1(3)} \end{bmatrix} H_0 \tag{III-12}$$

Equation (III-1) can be expressed in vehicle coordinates so that the torque applied to the vehicle becomes

$$\vec{T} = \left\{\frac{d\vec{H}}{dt}\right\}_{\text{vehicle space}} + \vec{\Omega} \times \vec{H} = \dot{\vec{H}} + \vec{\Omega} \times \vec{H} \qquad \text{(III-13)}$$

where $\vec{H}$ is as defined in Equation (III-12) and $\vec{\Omega}$ is the total angular velocity of the spacecraft

$$\vec{\Omega} = \begin{bmatrix} \Omega_x \bar{I}_i \\ \Omega_y \bar{I}_j \\ \Omega_z \bar{I}_k \end{bmatrix} \qquad \text{(III-14)}$$

$\dot{\vec{H}}$ indicates the time derivative of $\vec{H}$ with respect to vehicle space. Substituting the expressions for $\vec{H}$ given by Equation (III-12) and performing the indicated differentiation and cross-product operations yield

$$\vec{T} = D\dot{\vec{\delta}} + E\vec{\Omega} \qquad \text{(III-15)}$$

where

$$D = H_0 \begin{bmatrix} -S\delta_{3(1)}C\delta_{1(1)} & -C\delta_{3(1)}S\delta_{1(1)} & -C\delta_{3(2)}C\delta_{1(2)} \\ 0 & C\delta_{1(1)} & -S\delta_{3(2)}C\delta_{1(2)} \\ -C\delta_{3(1)}C\delta_{1(1)} & S\delta_{3(1)}C\delta_{1(1)} & 0 \end{bmatrix}$$

$$\begin{bmatrix} S\delta_{3(2)}S\delta_{1(2)} & 0 & C\delta_{1(3)} \\ -C\delta_{3(2)}S\delta_{1(2)} & -C\delta_{3(3)}C\delta_{1(3)} & S\delta_{3(3)}S\delta_{1(3)} \\ C\delta_{1(2)} & -S\delta_{3(3)}C\delta_{1(3)} & -C\delta_{3(3)}S\delta_{1(3)} \end{bmatrix} \qquad \text{(III-16)}$$

$$E = \begin{bmatrix} 0 & H_z & -H_y \\ -H_z & 0 & H_x \\ H_y & -H_x & 0 \end{bmatrix} \qquad \text{(III-17)}$$

and

$$\dot{\vec{\delta}} = \begin{bmatrix} \dot{\delta}_{3(1)} \\ \dot{\delta}_{1(1)} \\ \dot{\delta}_{3(2)} \\ \dot{\delta}_{1(2)} \\ \dot{\delta}_{3(3)} \\ \dot{\delta}_{1(3)} \end{bmatrix} \qquad \text{(III-18)}$$

B. Some Basic Approaches to CMG Steering Laws.

Basic CMG steering laws are concerned with commanding gimbal rates that will cause the moment exerted on the vehicle by the CMGs to reproduce the commanded torque as nearly as possible. The general form of vehicle attitude control using CMGs is shown in Figure III-5. The analysis will consider the CMGs to be free of any gimbal stops. The steering laws considered in this section assume that a vehicle control law to generate the commanded torque is available. Simulation results are presented in Chapter V for the steering laws presented in this section.

Since the D matrix is not a square matrix, it does not have an inverse and Equation (III-15) cannot be solved for $\dot{\vec{\delta}}$ exactly. The problem is to take any three-dimensional torque vector command $\vec{T}_c$ and develop a six-dimensional gimbal rate vector command $\dot{\vec{\delta}}_c$ for the CMG

torque motors. As pointed out by Ross in [3], one obvious solution to Equation (III-15) is

$$\dot{\vec{\delta}}_c = D^{\textcircled{-1}}(\vec{T}_c - E\vec{\Omega}) \tag{III-19}$$

where $D^{\textcircled{-1}}$ represents a matrix which satisfies the following equation

$$DD^{\textcircled{-1}} = I \tag{III-20}$$

where I is the identity matrix. There are an infinite number of $D^{\textcircled{-1}}$ matrices which satisfy this relationship. For example, partitioning the D matrix so that it can be expressed as

$$D = [D_1 \mid D_2] \tag{III-21}$$

suggests that a possible solution to Equation (III-20) is

$$D^{\textcircled{-1}} = \tfrac{1}{2}\begin{bmatrix} D_1^{-1} \\ D_2^{-1} \end{bmatrix} \tag{III-22}$$

This solution is valid for those orientations where the D_1 and D_2 matrices are nonsingular.

The above concept can be extended to the case where the solution to Equation (III-15) is

$$\dot{\vec{\delta}}_c = D^{-I}(\vec{T}_c - E\vec{\Omega}) \tag{III-23}$$

where D^{-I} is the pseudoinverse of D. D^{-I} can be chosen to be the pseudoinverse that gives the solution for the commanded gimbal rates with

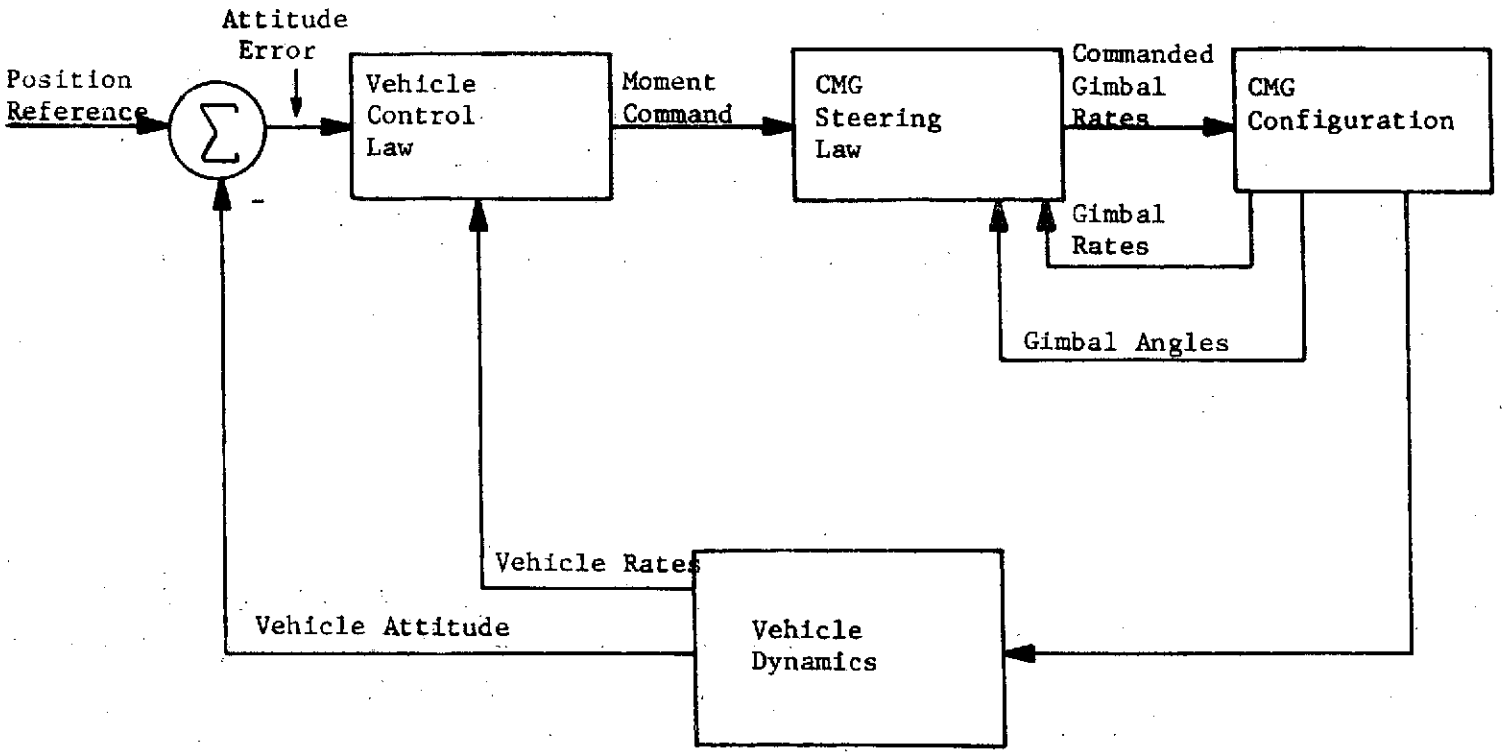

Figure III-5. Vehicle attitude control with control moment gyros.

the minimum norm if the solution is not unique [4]. This can be thought of as the $\dot{\vec{\delta}}$ vector that has the minimum length of all possible solutions. This technique does not depend on any matrices being non-singular.

It is desirable to design a control scheme that would minimize the amount of control effort required to achieve a given quality of control. One approach [5] is to find the law which minimizes a performance index such as

$$J = \sum_{\substack{i=1,3 \\ j=1,2,3}} \dot{\delta}^2_{i(j)} q_i + \sum_{k=x,y,z} (T_{ck} - T_k)^2 \qquad \text{(III-24)}$$

The q_i's relatively weight the control effort desired from the inner and outer torque motors with respect to the quality of control. In order to obtain an algebraic control law in terms of system parameters, the performance index is presented in terms of summations. This evaluates the system on a point-by-point basis in time which indicates that this law actually places a stronger constraint on the system than the integral performance measure which evaluates the system performance on an average basis. Expressing Equation (III-24) in vector form gives

$$J = \dot{\vec{\delta}}^T \hat{Q} \dot{\vec{\delta}} + (\vec{T}_c - \vec{T})^T (\vec{T}_c - \vec{T}) \qquad \text{(III-25)}$$

Substituting Equation (III-15) into (III-25) yields

$$J = \dot{\vec{\delta}}^T \hat{Q} \dot{\vec{\delta}} + (\vec{T}_c - D\dot{\vec{\delta}} - E\vec{\Omega})^T(\vec{T}_c - D\dot{\vec{\delta}} - E\vec{\Omega})$$

$$= \dot{\vec{\delta}}^T \hat{Q} \dot{\vec{\delta}} + \vec{T}_c^T \vec{T} - \vec{T}_c^T D\dot{\vec{\delta}} - \vec{T}_c^T E\vec{\Omega} - \dot{\vec{\delta}}^T D^T \vec{T}_c + \dot{\vec{\delta}}^T D^T D\dot{\vec{\delta}}$$

$$+ \dot{\vec{\delta}}^T D^T E\vec{\Omega} - \vec{\Omega}^T E^T \vec{T}_c + \vec{\Omega}^T E^T D\dot{\vec{\delta}} + \vec{\Omega}^T E^T E\vec{\Omega}$$

(III-26)

In order to minimize J, the partial derivative $\partial J/\partial \dot{\vec{\delta}}^T$ must be equated to the zero vector. Simplifying this expression yields

$$\frac{\partial J}{\partial \dot{\vec{\delta}}^T} = \left[\hat{Q} \dot{\vec{\delta}} - D^T(\vec{T}_c - E\vec{\Omega}) + D^T D \dot{\vec{\delta}}\right] 2 = 0 \qquad \text{(III-27)}$$

Solving Equation (III-27) for $\dot{\vec{\delta}}$ gives

$$\dot{\vec{\delta}}_c = [\hat{Q} + D^T D]^{-1} D^T(\vec{T}_c - E\vec{\Omega}) \qquad \text{(III-28)}$$

$\hat{Q}$ is the positive definite weighting matrix determining the relative control effort of the inner and outer gimbal torque motors. Defining $\hat{Q}^{-1}$ as K_{SL}, the steering law gain, and referring to Equation (III-24), it is observed that increasing K_{SL} will increase the quality of control at the expense of higher gimbal rates. Figure III-6 shows a scheme to realize this CMG control law with D^T referred to as the "Transpose Steering Law" [3].

The above steering laws have not considered the problem of gimbal stops or antiparallel orientations. While the laws can be modified to protect against these conditions, this is not considered in this

investigation. The basic steering laws developed in this chapter from the CMG equations of motion are compared to a total optimal CMG control law (presented in Chapter IV) in Chapter V.

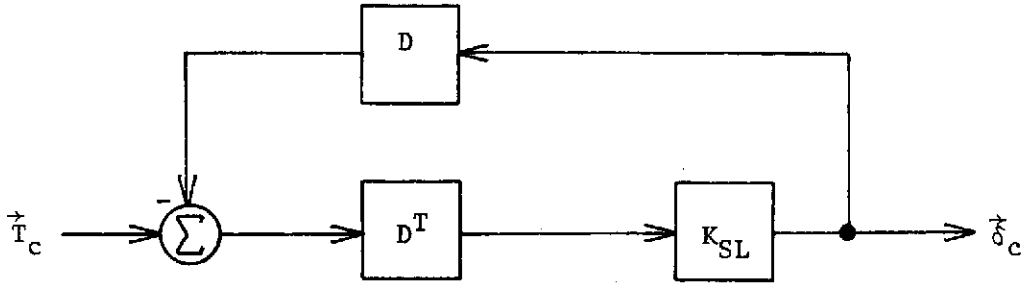

Figure III-6. A scheme to implement the transpose steering law.

IV. A TOTAL OPTIMAL CMG ATTITUDE CONTROL LAW

The steering laws presented in Chapter III assumed that a controller provided a commanded torque as input to the CMG steering law. In this chapter a control law is developed that commands the CMG gimbal rates based on the input of the attitude error angles and the error rates. The variables of the non-linear, multi-input, multi-output CMG system are treated in a special way so that the tools of linear system theory can be applied to this problem. The feedback control policy is determined using the state variable approach and optimal control theory. The development of this control policy utilizes Kalman's work showing that the optimal control for a non-linear system can be given by the solution of the optimization problem for a set of system equations linearized about the current operating point [6].

The system presented in this chapter is a special case of the one developed by Skelton in [7] using the concepts described above. The system presented here differs in that the gyros are considered to be free of gimbal stops and the problem of antiparallel orientations is not considered. The result of applying this approach is a closed loop law that generates the six gimbal rate commands as a linear combination of the vehicle rates and vehicle attitudes. The gains multiplying these variables are updated as a function of the changes in the gimbal angles.

The states of the system are chosen to be the attitude errors, vehicle rate errors, and gimbal angles so that

$$\begin{bmatrix} x_1 \\ x_2 \\ x_3 \end{bmatrix} = \begin{bmatrix} \theta_1 \\ \theta_2 \\ \theta_3 \end{bmatrix} = \vec{\theta} \qquad \text{(IV-1)}$$

$$\begin{bmatrix} x_4 \\ x_5 \\ x_6 \end{bmatrix} = \begin{bmatrix} \Omega_1 \\ \Omega_2 \\ \Omega_3 \end{bmatrix} = \vec{\Omega} \qquad \text{(IV-2)}$$

and

$$\begin{bmatrix} x_7 \\ x_8 \\ x_9 \\ x_{10} \\ x_{11} \\ x_{12} \end{bmatrix} = \begin{bmatrix} \delta_{1(1)} \\ \delta_{1(2)} \\ \delta_{1(3)} \\ \delta_{3(1)} \\ \delta_{3(2)} \\ \delta_{3(3)} \end{bmatrix} = \vec{\delta} \qquad \text{(IV-3)}$$

The gimbal rates are chosen as the control vector so that

$$\begin{bmatrix} u_1 \\ u_2 \\ u_3 \\ u_4 \\ u_5 \\ u_6 \end{bmatrix} = \begin{bmatrix} \dot{\delta}_{1(1)} \\ \dot{\delta}_{1(2)} \\ \dot{\delta}_{1(3)} \\ \dot{\delta}_{3(1)} \\ \dot{\delta}_{3(2)} \\ \dot{\delta}_{3(3)} \end{bmatrix} = \dot{\vec{\delta}} \qquad \text{(IV-4)}$$

For the SIXPAC CMG system, the equation for the vehicle can be written as

$$\dot{\vec{\Omega}} = J^{-1} \left[D\dot{\vec{\delta}} + E\vec{\Omega} - \vec{\Omega} \times J \cdot \vec{\Omega} + \vec{T}_{ex} \right] \qquad \text{(IV-5)}$$

where $\vec{T}_{ex}$ = the external torque applied to the vehicle

J = the inertia dyadic of the vehicle

and D, E, $\vec{\delta}$, and $\vec{\Omega}$ are as described in Chapter III.

When the primary external torque is due to gravity gradient, it is shown in [8] that this torque can be expressed as

$$\vec{T}_{ex} = \vec{T}_n(t) + G(t)\,\vec{\theta} \qquad \text{(IV-6)}$$

where $\vec{T}_n(t)$ is a time dependent gravity gradient torque evaluated at a nominal attitude and the elements of the G matrix are the first order partial derivatives of the torque with respect to θ and evaluated at the nominal θ.

The components of the body rates can be related to the Euler angle rates by manipulating the transformation from inertial space to vehicle space. If the Euler sequence of rotations is 1, 2, 3, then the vehicle reference frame $(\vec{v})$ may be related to the inertial reference frame $(\vec{z})$ as

$$\vec{v} = \theta\vec{z} = [{}^3\theta]\,[{}^2\theta]\,[{}^1\theta]\,\vec{z} \qquad \text{(IV-7)}$$

where

$$[{}^1\theta] = \begin{bmatrix} 1 & 0 & 0 \\ 0 & \cos\theta_1 & \sin\theta_1 \\ 0 & -\sin\theta_1 & \cos\theta_1 \end{bmatrix} \qquad \text{(IV-8a)}$$

$$ {}^{2}\theta = \begin{bmatrix} \cos\theta_2 & 0 & -\sin\theta_2 \\ 0 & 1 & 0 \\ \sin\theta_2 & 0 & \cos\theta_2 \end{bmatrix} \qquad \text{(IV-8b)} $$

$$ {}^{3}\theta = \begin{bmatrix} \cos\theta_3 & \sin\theta_3 & 0 \\ -\sin\theta_3 & \cos\theta_3 & 0 \\ 0 & 0 & 1 \end{bmatrix} \qquad \text{(IV-8c)} $$

Therefore, using Equations (IV-8) in Equation (IV-7), the elements of θ are determined to be

$$
\begin{aligned}
\theta_{11} &= \cos\theta_2\cos\theta_3 \\
\theta_{12} &= \cos\theta_1\sin\theta_3 + \sin\theta_1\sin\theta_2\cos\theta_3 \\
\theta_{13} &= \sin\theta_1\sin\theta_3 - \cos\theta_1\sin\theta_2\cos\theta_3 \\
\theta_{21} &= -\cos\theta_2\sin\theta_3 \\
\theta_{22} &= \cos\theta_1\cos\theta_3 - \sin\theta_1\sin\theta_2\sin\theta_3 \\
\theta_{23} &= \sin\theta_1\cos\theta_3 + \cos\theta_1\sin\theta_2\sin\theta_3 \\
\theta_{31} &= \sin\theta_2 \\
\theta_{32} &= -\sin\theta_1\cos\theta_2 \\
\theta_{33} &= \cos\theta_1\cos\theta_2
\end{aligned}
\qquad \text{(IV-9)}
$$

It should be noted that the ${}^1\theta$, ${}^2\theta$, ${}^3\theta$, and θ matrices are unitary matrices which means that their inverse is equal to their transpose. This property is used below to get an expression for the vehicle angular velocity. The angular velocity of the vehicle can be expressed in terms of the Euler rates as

$$\vec{\Omega} = \dot{\theta}_1 z_1 + \dot{\theta}_2 v_2' + \dot{\theta}_3 v_3$$

$$= [z_1, v_2', v_3] \begin{bmatrix} \dot{\theta}_1 \\ \dot{\theta}_2 \\ \dot{\theta}_3 \end{bmatrix} \qquad \text{(IV-10)}$$

where $\vec{v}'$ is an intermediate coordinate system. Equation (IV-7) can alternately be expressed as

$$\begin{bmatrix} v_1 \\ v_2 \\ v_3 \end{bmatrix} = z_1 \begin{bmatrix} \theta_{11} \\ \theta_{21} \\ \theta_{31} \end{bmatrix} + z_2 \begin{bmatrix} \theta_{12} \\ \theta_{22} \\ \theta_{32} \end{bmatrix} + z_3 \begin{bmatrix} \theta_{13} \\ \theta_{23} \\ \theta_{33} \end{bmatrix} \qquad \text{(IV-11)}$$

The intermediate coordinate system $\vec{v}'$ is

$$\vec{v}' = [{}^1\theta]\vec{z} = [{}^1\theta]\theta^T\vec{v} \qquad \text{(IV-12)}$$

Then solving for $\vec{v}$ in terms of $\vec{v}'$ in Equation (IV-12) yields

$$\vec{v} = \theta[{}^1\theta^T]\vec{v}' \qquad \text{(IV-13)}$$

Using Equations (IV-8a) and (IV-9) and performing the indicated matrix multiplications in Equation (IV-13) yields

$$\begin{bmatrix} v_1 \\ v_2 \\ v_3 \end{bmatrix} = v_1' \begin{bmatrix} \theta_{11} \\ \theta_{21} \\ \theta_{31} \end{bmatrix} + v_2' \begin{bmatrix} \sin\theta_3 \\ \cos\theta_3 \\ 0 \end{bmatrix} + v_3' \begin{bmatrix} \theta_{13}\cos\theta_1 - \theta_{12}\sin\theta_1 \\ \theta_{23}\cos\theta_1 - \theta_{22}\sin\theta_1 \\ \theta_{33}\cos\theta_1 - \theta_{32}\sin\theta_1 \end{bmatrix} \tag{IV-14}$$

Finally, the vehicle coordinate system can also be expressed as

$$\begin{bmatrix} v_1 \\ v_2 \\ v_3 \end{bmatrix} = v_1 \begin{bmatrix} 1 \\ 0 \\ 0 \end{bmatrix} + v_2 \begin{bmatrix} 0 \\ 1 \\ 0 \end{bmatrix} + v_3 \begin{bmatrix} 0 \\ 0 \\ 1 \end{bmatrix} \tag{IV-15}$$

Therefore, from Equations (IV-10), (IV-11), (IV-14), and (IV-15) the expression for the vehicle rates becomes

$$\begin{bmatrix} \Omega_1 \\ \Omega_2 \\ \Omega_3 \end{bmatrix} = \begin{bmatrix} \cos\theta_2\cos\theta_3 & \sin\theta_3 & 0 \\ -\cos\theta_2\sin\theta_3 & \cos\theta_3 & 0 \\ \sin\theta_2 & 0 & 1 \end{bmatrix} \begin{bmatrix} \dot{\theta}_1 \\ \dot{\theta}_2 \\ \dot{\theta}_3 \end{bmatrix} \tag{IV-16}$$

Solving Equation (IV-16) for the Euler angle rates yields

$$\begin{bmatrix} \dot{\theta}_1 \\ \dot{\theta}_2 \\ \dot{\theta}_3 \end{bmatrix} = \begin{bmatrix} \cos\theta_3 / \cos\theta_2 & -\sin\theta_3/\cos\theta_2 & 0 \\ \sin\theta_3 & \cos\theta_3 & 0 \\ -\tan\theta_2\cos\theta_3 & \tan\theta_2\sin\theta_3 & 1 \end{bmatrix} \begin{bmatrix} \Omega_1 \\ \Omega_2 \\ \Omega_3 \end{bmatrix} \tag{IV-17}$$

Equations (IV-5) and (IV-17) describe the dynamics of the system to be controlled. These equations are expressed in terms of the state variables defined in Equations (IV-1) through (IV-4) as

$$\begin{bmatrix} \dot{x}_1 \\ \dot{x}_2 \\ \dot{x}_3 \end{bmatrix} = W(x_2, x_3) \begin{bmatrix} x_4 \\ x_5 \\ x_6 \end{bmatrix} \tag{IV-18}$$

where W is as given in Equation (IV-17) with θ_2 and θ_3 replaced by x_2 and x_3 respectively, and

$$\begin{bmatrix} \dot{x}_4 \\ \dot{x}_5 \\ \dot{x}_6 \end{bmatrix} = J^{-1} \left\{ D(\vec{\delta})\dot{\vec{u}} + E \begin{bmatrix} x_4 \\ x_5 \\ x_6 \end{bmatrix} - \begin{bmatrix} x_4 \\ x_5 \\ x_6 \end{bmatrix} \times J \cdot \begin{bmatrix} x_4 \\ x_5 \\ x_6 \end{bmatrix} + \vec{T}_n(t) + G \begin{bmatrix} x_1 \\ x_2 \\ x_3 \end{bmatrix} \right\} \tag{IV-19}$$

and

$$\begin{bmatrix} \dot{x}_7 \\ \dot{x}_8 \\ \dot{x}_9 \\ \dot{x}_{10} \\ \dot{x}_{11} \\ \dot{x}_{12} \end{bmatrix} = \begin{bmatrix} u_1 \\ u_2 \\ u_3 \\ u_4 \\ u_5 \\ u_6 \end{bmatrix} \tag{IV-20}$$

Equations (IV-18) through (IV-20) are of the general form

$$\dot{\vec{x}} = \vec{f}(\vec{x}, \vec{u}, t) \tag{IV-21}$$

Expanding Equation (IV-21) about the nominal operating point, $\vec{x}_{nom}$ and $\vec{u}_{nom}$, into the Taylor Series for $\dot{\vec{x}}$ yields

$$\dot{\vec{x}} = \vec{f}(\vec{x}_{nom}, \vec{u}_{nom}, t) + \left.\frac{\partial \vec{f}}{\partial \vec{x}}\right|_{\substack{\vec{x}=\vec{x}_{nom} \\ \vec{u}=\vec{u}_{nom}}} (\vec{x} - \vec{x}_{nom}) + \left.\frac{\partial \vec{f}}{\partial \vec{u}}\right|_{\substack{\vec{x}=\vec{x}_{nom} \\ \vec{u}=\vec{u}_{nom}}} (\vec{u} - \vec{u}_{nom})$$

$$+ \vec{g}(\vec{x} - \vec{x}_{nom}, \vec{u} - \vec{u}_{nom}, t) \qquad \text{(IV-22)}$$

where $\vec{g}$ contains the higher order terms.

Defining

$$\vec{y} = \vec{x} - \vec{x}_{nom}$$

and $$\vec{v} = \vec{u} - \vec{u}_{nom} \qquad \text{(IV-23)}$$

the general form of the linearized equations is

$$\dot{\vec{y}} = A\vec{y} + B\vec{v} \qquad \text{(IV-24)}$$

where $$A_{ij} = \left.\frac{\partial f_i}{\partial x_j}\right|_{\substack{\vec{x}=\vec{x}_{nom} \\ \vec{u}=\vec{u}_{nom}}} \quad \text{and} \quad B_{ij} = \left.\frac{\partial f_i}{\partial u_j}\right|_{\substack{\vec{x}=\vec{x}_{nom} \\ \vec{u}=\vec{u}_{nom}}}$$

The steady state gimbal rate, $\vec{u}_{nom}$, is obtained as the equilibrium solution of Equation (IV-5), (i.e. $\dot{\vec{\Omega}} = \vec{\Omega} = 0$), as

$$\vec{u}_{nom} = D^{-I}(\vec{T}_n + G\vec{\theta}) \qquad \text{(IV-25)}$$

where D^{-I} is the pseudoinverse of the nonsquare D matrix and Equation (IV-6) has been substituted into Equation (IV-5). $\vec{u}_{nom}$ is considered a constant in Equation (IV-25) since the time constants of the gravity gradient torques are large compared to the time constants of the

stabilized control system.

It is desirable to keep the average attitude and rate errors small as well as prevent excessive peak errors in attitude and rate. Therefore, the performance measure for the optimal system penalizes position and rate terms to avoid excessively large control efforts. Since gimbal stops are not considered here, there is no reason to penalize the gimbal angles. The performance measure is

$$P(\vec{\dot{\delta}}) = \int_0^T \tfrac{1}{2} \left\{ \vec{\theta}_e^T L \vec{\theta}_e + \vec{\Omega}^T J \vec{\Omega} + \vec{\dot{\delta}}_e^T R \vec{\dot{\delta}}_e \right\} dt \qquad \text{(IV-26)}$$

where $\vec{\theta}_e = \vec{\theta} - \vec{\theta}_{command} = \vec{\theta} - \vec{\theta}_{nom}$

and $\vec{\dot{\delta}}_e = \vec{\dot{\delta}} - \vec{\dot{\delta}}_{nom}$

Since $\vec{\Omega}_{nom} = 0$, Equation (IV-26) can be written in terms of the defined state variables as

$$P(\vec{u}) = \int_0^T \tfrac{1}{2} \left\{ \vec{y}^T Q \vec{y} + \vec{v}^T R \vec{v} \right\} dt \qquad \text{(IV-27)}$$

where

$$Q = \begin{bmatrix} L_{3x3} & 0_{3x3} & 0_{3x3} \\ 0_{3x3} & J_{3x3} & 0_{3x3} \\ 0_{3x3} & 0_{3x3} & 0_{3x3} \end{bmatrix}$$

and

$$R = \begin{bmatrix} r_1 & 0 & 0 & 0 & 0 & 0 \\ 0 & r_2 & 0 & 0 & 0 & 0 \\ 0 & 0 & r_3 & 0 & 0 & 0 \\ 0 & 0 & 0 & r_4 & 0 & 0 \\ 0 & 0 & 0 & 0 & r_5 & 0 \\ 0 & 0 & 0 & 0 & 0 & r_6 \end{bmatrix}$$

The term $\vec{\Omega}^T J \vec{\Omega}$ represents the vehicle kinetic energy and minimizing the integral of the vehicle kinetic energy conserves vehicle energy expenditure. L and R elements are generally chosen smaller than J because of this aspect of energy conservation.

Kalman shows in [6] that a system described by Equation (IV-24) minimizes a functional of the form of Equation (IV-27) (where Q is any positive semi-definite matrix and R is any positive definite matrix) subject to the constraints

$$\vec{y}(0) = \vec{y}_o$$

$$\vec{y}(\infty) = \text{unspecified}$$

when

$$\vec{v} = -R^{-1}B^T K \vec{y} \qquad \text{(IV-28)}$$

where K is the symmetric, positive definite gain matrix that is the solution to the matrix Riccati equation

$$\dot{K} = -KA - A^T K - Q + KBR^{-1}B^T K \qquad \text{(IV-29)}$$

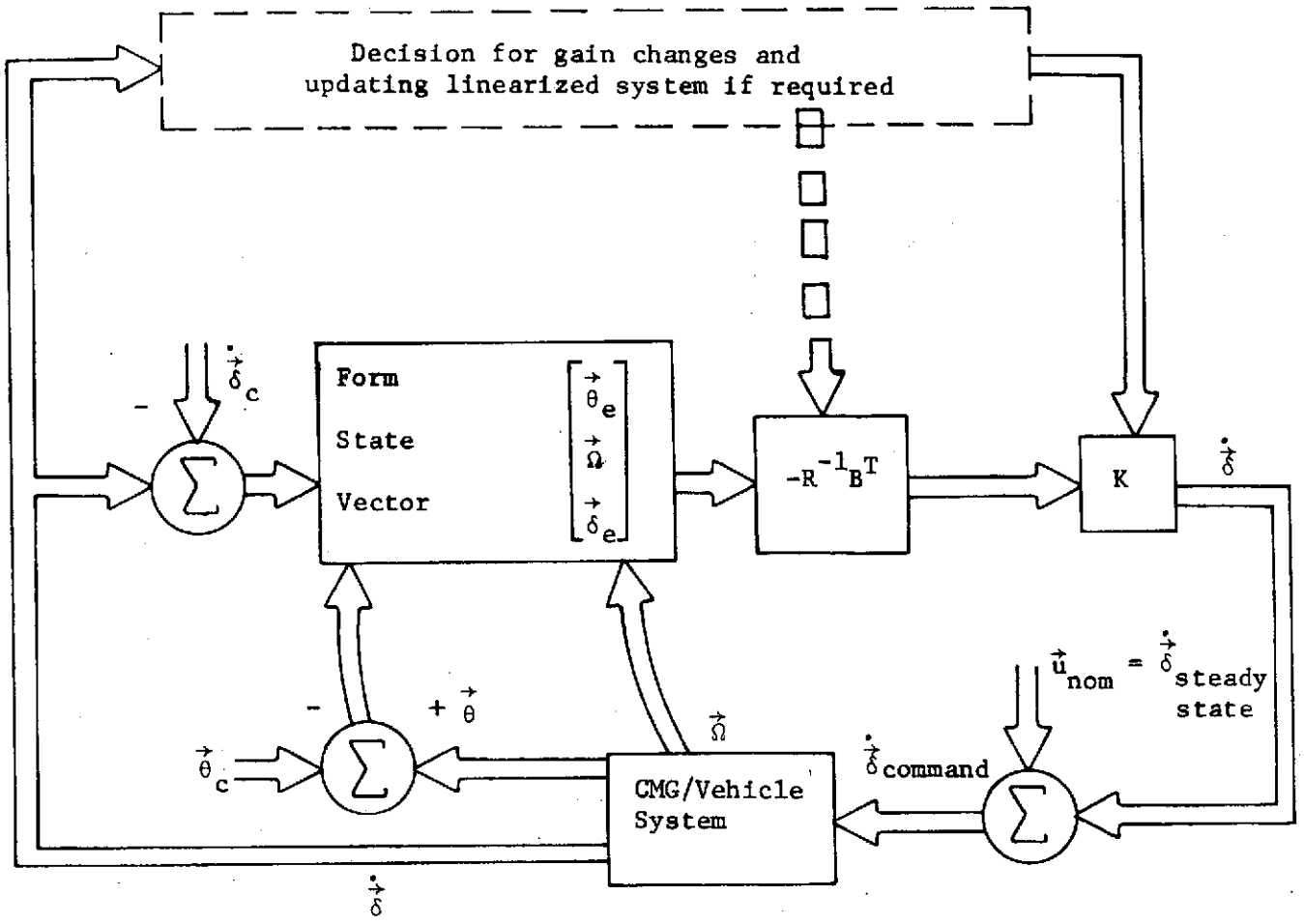

Figure IV-1. An implementation of the sub-optimal control system.

Equations (IV-28) and (IV-29) give the optimal solution if the system given by Equation (IV-24) is completely controllable. If the system is not completely controllable, the solution is optimal only when the uncontrollable states are not penalized.

The solution to the linear regulator problem is the solution to the non-linear plant if the linearized model is updated frequently. The linearized model must be updated as a function of time, gimbal angles, and vehicle attitude commands. The gimbal angles will be the fastest to change and usually can provide the criterion for updating the linearized model. Equations (IV-28) and (IV-29) give a sub-optimal solution as a result of the frequent updating of the linearized model, but if the updating period is long compared to the system time constants, then this solution approaches the optimal. An implementation of this sub-optimal control system is shown in Figure IV-1.

A. Sensitivity Analysis of the Riccati Equation

A difficulty in implementing the optimal control system given by Equations (IV-28) and (IV-29) centers about finding the steady state solution to the matrix Riccati equation given by Equation (IV-29). Problems encountered are excessive computation time for the desired accuracy of the Riccati equation solution. Two approaches are considered to decrease the degree of these difficulties. First a sensitivity analysis of the gains with respect to the gimbal angles is performed to determine if some gains may be considered constant. Those constant

gains would not have to be computed at each linearization update, thus saving on computation time. In Section B different solution techniques are evaluated with respect to computation time and accuracy to determine which solution method is most acceptable with respect to these requirements.

As is pointed out by Skelton in [7], it is sufficient to solve the sixth order Riccati equation when the gimbal angles are not penalized. The reduced sixth order system is

$$\begin{bmatrix} x_{1-3} \\ x_{4-6} \end{bmatrix} = \begin{bmatrix} 0 & W \\ 0 & A_2 \end{bmatrix} \begin{bmatrix} x_{1-3} \\ x_{4-6} \end{bmatrix} + \begin{bmatrix} 0 \\ B_1 \end{bmatrix} \vec{u} \qquad \text{(IV-30)}$$

where W is given in Equation (IV-17)

$$A_2 = J^{-1} \begin{bmatrix} 0 & -h_3 & h_2 \\ h_3 & 0 & -h_1 \\ -h_2 & h_1 & 0 \end{bmatrix}$$

$$B_1 = J^{-1} D \Big|_{\vec{x}=\vec{x}_{nom}}$$

and J is the inertia dyadic of the vehicle. Since the gimbal angles are not penalized in the performance measure, only the sixth order case will be considered here.

Rewriting Equation (IV-29) in the steady state and showing explicit dependence on a parameter α yields

$$A^T(\alpha)K(\alpha) + K(\alpha) - K(\alpha)S(\alpha)K(\alpha) + Q = 0 \qquad \text{(IV-31)}$$

where $S(\alpha) = B(\alpha)R^{-1}B^T(\alpha)$

Taking the partial of Equation (IV-31) with respect to α gives

$$\frac{\partial A^T}{\partial \alpha} K + A^T \frac{\partial K}{\partial \alpha} + \frac{\partial K}{\partial \alpha} A + K \frac{\partial A}{\partial \alpha} - \frac{\partial K}{\partial \alpha} SK - K \frac{\partial S}{\partial \alpha} K - KS \frac{\partial K}{\partial \alpha} = 0 \tag{IV-32}$$

Combining like terms simplifies Equation (IV-32) to

$$\frac{dK}{d\alpha} (A - SK) + (A - SK)^T \frac{dK}{d\alpha} = -K\eta - \eta^T K + K\delta K \tag{IV-33}$$

where $\eta = dA/d\alpha$

$\delta = dS/d\alpha$

and with all matrices evaluated at $\alpha = \alpha_0$. The form of Equation (IV-33) is

$$FG + G^T F + H = 0 \tag{IV-34}$$

where $F = dK/d\alpha$

$G = A - SK$

and $H = K\eta + \eta^T K - K\delta K$

Kleinman presents an algorithm in [9] that is used to iteratively solve equations of the same form as Equation (IV-34) numerically. The steady state Riccati solution for several initial gimbal angle configurations ($K(\alpha_0)$) is computed here; then Equation (IV-34) is iteratively solved for $dK/d\alpha$ using Kleinman's algorithm. The percentage variation in K for a $\Delta\alpha$ change in a gimbal angle is approximated as

$$S_{\alpha}^{K} = \frac{dK}{d\alpha} \frac{\Delta\alpha}{K} \qquad \text{(IV-35)}$$

where S_{α}^{K} is the sensitivity of K with respect to parameter α

α is a gimbal angle, $\alpha = \delta_1, \delta_2, \ldots\delta_6$

and $\Delta\alpha$ is the incremental change in the gimbal angle α.

Performing these operations for gimbal angle orientations that are combinations of 0° and 30° gimbal angles is sufficient to indicate that no gains are insensitive enough to gimbal angle variations to consider them constant.

The diagonal elements of the steady-state solution to the Riccati equation are generally much less sensitive to gimbal angle variations than are the off-diagonal terms. Table IV-1 gives the range of the values of the off-diagonal terms of the gain matrix for the various gimbal angle configurations that are considered. For these same cases, Table IV-2 gives the range of the sensitivities of these off-diagonal terms to 5° incremental changes in the δ_1 gimbal angle. Results are presented only for the δ_1 gimbal angle sensitivity because these results are typical of those obtained for the sensitivities of these elements to the other five gimbal angles. Since Table IV-2 indicates the extreme sensitivity of the off-diagonal terms to gimbal angle variations, only the diagonal terms can possibly be insensitive enough to gimbal angle variations to be considered constant.

The range of the values of the Riccati gain matrix diagonal terms are given in Table IV-3 for the different gimbal angle configurations analyzed. Table IV-4 describes the range of the maximum

Table IV-1. Range of Riccati Gain Matrix Off-Diagonal Elements For Several Combinations of 0° and 30° Gimbal Angles.

Gain Matrix Element	Range of Matrix Element Values	
	Max	Min
K_{12}	1.75×10^{4}	-4.32×10^{4}
K_{13}	5.27×10^{3}	-4.30×10^{4}
K_{14}	2.51×10^{5}	1.55×10^{5}
K_{15}	6.09×10^{4}	-1.51×10^{5}
K_{16}	1.91×10^{4}	-1.49×10^{5}
K_{23}	4.34×10^{4}	-8.03×10^{4}
K_{24}	6.14×10^{4}	-1.49×10^{5}
K_{25}	1.60×10^{6}	1.28×10^{6}
K_{26}	1.55×10^{5}	-2.86×10^{5}
K_{34}	1.83×10^{4}	-1.49×10^{5}
K_{35}	1.56×10^{5}	-2.85×10^{5}
K_{36}	1.84×10^{6}	1.27×10^{6}
K_{45}	2.52×10^{5}	-6.08×10^{5}
K_{46}	7.84×10^{4}	-6.06×10^{5}
K_{56}	6.67×10^{5}	-1.20×10^{6}

Table IV-2. Range of Sensitivity of Riccati Gain Matrix Off-Diagonal Elements to Variations in δ_1 Gimbal Angle For Several Combinations of 0° and 30° Gimbal Angles. 5° Variation in δ_1 is Used.

Gain Matrix Element	Range of Sensitivity of Matrix Element Values (Absolute Value)	
	Max	Min
K_{12}	7.77×10^{5}	4.42×10^{-3}
K_{13}	2.43×10^{6}	3.05×10^{-1}
K_{14}	9.81	7.74×10^{-4}
K_{15}	2.79×10^{4}	2.11×10^{-2}
K_{16}	7.36×10	2.73×10^{-1}
K_{23}	4.33×10^{4}	7.83×10^{-3}
K_{24}	2.39×10^{3}	1.23×10^{-2}
K_{25}	1.53	2.09×10^{-6}
K_{26}	1.35×10^{4}	1.54×10^{-2}
K_{34}	9.55×10^{3}	1.12×10^{-1}
K_{35}	8.41×10^{3}	5.89×10^{-4}
K_{36}	2.74	1.01×10^{-3}
K_{45}	4.04×10^{5}	3.23×10^{-3}
K_{46}	1.22×10^{8}	4.37×10^{-2}
K_{56}	5.79×10^{4}	1.68×10^{-3}

Table IV-3. Range of Riccati Gain Matrix Diagonal Elements For Several Combinations of 0° and 30° Gimbal Angles.

Gain Matrix Element	Range of Matrix Element Values	
	Max	Min
K_{11}	3.83×10^5	3.54×10^5
K_{22}	2.39×10^6	2.30×10^6
K_{33}	2.43×10^6	2.28×10^6
K_{44}	8.89×10^5	5.10×10^5
K_{55}	5.78×10^6	4.41×10^6
K_{66}	6.84×10^6	4.38×10^6

Table IV-4. Range of Maximum Value of Sensitivities (for 5° Gimbal Angle Increments) of Gain Matrix Diagonal Elements to the Six Gimbal Angles.

Gain Matrix Element	Range of Sensitivity of Matrix Element Values (Absolute Value)	
	Max	Min
K_{11}	1.30	2.93×10^{-2}
K_{22}	2.93	1.79×10^{-1}
K_{33}	1.47	1.93×10^{-1}
K_{44}	4.66	3.94×10^{-1}
K_{55}	5.86	1.25
K_{66}	4.81	1.27

sensitivities of these gain elements with respect to variations in the six gimbal angles. Table IV-4 illustrates that the diagonal terms are much less sensitive to the gimbal angles than the off-diagonal terms; however, it also indicates that no elements of the Riccati gain matrix are insensitive enough to the gimbal angles to be considered constant. As a consequence, all elements of the gain matrix must be computed at each linearization update and no computational time can be saved by considering some elements to be constant.

These results were obtained by using the same system as Skelton in [7]. Therefore, the procedure employed in this section should be employed for the system under consideration. If an element of the gain matrix is determined to be insensitive to given parameter variations within a specified degree, then that element may be considered constant thus reducing required computational time.

B. Numerical Solution Techniques for the Riccati Equation

A conventional Runge-Kutta integration scheme is used in [7] to solve Equation IV-29 for K in the steady state. Some other numerical techniques are considered here and compared to determine if another algorithm might give the Riccati gain matrix with less computational time and accuracy comparable to a Runge-Kutta method.

Two other integration algorithms, Euler and Modified Euler, are evaluated along with the Runge-Kutta scheme. These should have smaller computational times at a cost to the accuracy of the steady state solution.

Russell presents a mathematical technique in [11] that accelerates the convergance of a transient computer solution to steady state conditions thus substantially reducing execution time. This procedure is applicable when

(1) the boundary conditions and internal constraints are either constant or cyclic

(2) the steady state results are independent of the initial conditions, and

(3) only the steady state solution is desired.

There are two accelerations techniques -- exponential extrapolation and constant proportionality adjustment. Exponential extrapolation involves fitting an exponential curve through three points in the transient solution and predicting the steady state value. The general form of the fitting curve is given as

$$Y(t) = C_1 + C_2 e^{-C_3 t} \tag{IV-36}$$

Assuming the values of the three points along the transient solution to be Y_1, Y_2, and Y_3, then the steady state value for Y(t) in Equation (IV-36) is given as

$$Y(t = \infty) = \frac{Y_1 Y_3 - Y_2^2}{Y_1 + Y_3 - 2Y_2} \tag{IV-37}$$

The solution adjustment is obtained from Equation (IV-37) as

$$\Delta Y = \frac{Y_1 Y_3 - Y_2^2}{Y_1 + Y_3 - 2Y_2} - Y_1 \tag{IV-38}$$

The constant proportionality adjustment is

$$\Delta Y = SKIP\left[\frac{Y_2 - Y_1}{\Delta t}\right] \qquad \text{(IV-39)}$$

where SKIP is a constant multiplication factor input by the user. This method is usually less accurate than exponential extrapolation, but it usually requires less computation time as well as requiring less storage space.

Since the possibility of solution instability is enhanced with the accelerated integration techniques, the sign of the adjustment to the gain values can be checked. If the sign changes, then the incremental adjustment is modified by a constant reduction factor to prevent instability or at least to retard it. If the sign change is indicative of a simple overshoot rather than instability, the modification to the incremental adjustment should speed up the solution computationally.

In [9] and [12] Kleinman presents an iterative algebraic technique to solve for the linear regulator Riccati gain matrix. If V_k, k = 0, 1, ... is the unique positive definite solution of the linear algebraic equation

$$A_k^T V_k + V_k A_k + Q + L_k^T RL_k = 0 \qquad \text{(IV-40)}$$

where recursively,

$$L_k = R^{-1}B^T V_{k-1} \qquad k = 1, 2, \ldots \qquad \text{(IV-41)}$$

$$A_k = A - BL_k \qquad \text{(IV-42)}$$

and where L_0 is chosen such that the matrix $A_0 = A - BL_0$ has eigenvalues with negative real parts, then

$$K \leq V_{k+1} \leq V_k \leq \ldots \qquad k = 0, 1 \tag{IV-43}$$

and

$$\lim_{k \to \infty} V_k = K \tag{IV-44}$$

where K is the steady state solution to Equation (IV-29). Kleinman presents the computational algorithms to implement this procedure in [9].

A program for the Linear Quadratic Loss (LQL) problem [13] uses Potter's algebraic method [14] to obtain the steady state solution to the Riccati equation. Potter's method involves finding the eigenvectors (or pseudo eigenvectors) corresponding to eigenvalues with negative real parts of the 2n x 2n Hamiltonian matrix,

$$H = \begin{bmatrix} A & -BR^{-1}B^T \\ -Q & -A^T \end{bmatrix} \tag{IV-45}$$

Spectral factorization of the Hamiltonian matrix is used to obtain these eigenvalues. The stable eigenvectors are then used to form a 2n x n matrix whose columns are the real eigenvectors. If the eigenvectors are in complex conjugate pairs, two vectors made up of the real and imaginary parts of one of the complex eigenvectors are used instead of the complex entries. If this 2n x n matrix so formed is

$$\begin{bmatrix} D \\ E \end{bmatrix} \tag{IV-46}$$

then the steady state solution to the Riccati equation is determined to be

$$K = ED^{-1} \tag{IV-47}$$

Using the same system parameters as in [7], solutions to the Riccati equation are obtained using the previous algorithms. Since the algorithms would be programmed on a particular flight control computer, the actual computation times for these procedures would be meaningless. Therefore, the tabular results presented in the remainder of this chapter are normalized. The minimum value of the parameter for all cases considered is assigned the value zero while the maximum value is assigned the value 100. All intermediate values are assigned a value between 0 and 100 in the following linear fashion,

$$p_n = \left(\frac{p_i - p_{min}}{p_{max} - p_{min}} \right) 100 \tag{IV-48}$$

where p_n is the normalized parameter value,

p_i is the actual parameter value,

p_{min} is the minimum parameter value,

and p_{max} is the maximum parameter value.

Since the steady state solution to the Riccati equation is desired, the derivatives of each of the gains at the computed solution point gives a measure of the solution accuracy. For the results included in the remainder of this chapter, the accuracy comparison values are obtained by summing the absolute values of all the elements of the

gain derivative matrix. These values are then normalized according to Equation (IV-48).

Euler, Modified Euler, and Runge-Kutta integration procedures are examined in this analysis. Additionally, these solution techniques are examined with exponential acceleration and proportional acceleration, both with and without the instability retardation routine. Finally, the Kleinman and Potter algebraic routines are compared to the integration routines. Since a conventional Runge-Kutta integration algorithm is used in [7], this case is included in several of the following tables for the purpose of comparison.

The integration routines are very sensitive to the integration time increment. Table IV-5 illustrates the expected decrease in computational time for an increase in the integration time increment for the conventional Runge-Kutta integration solution.

For those cases including instability suppression, the value of the constant factor to modify the solution adjustment is chosen to be .1. This value represents a good choice, but not necessarily a best choice. Solutions to the Riccati equation are obtained using other values, but there is no general trend. In some instances .1 gives the better result with respect to computational time and accuracy, while in other instances .025 and .25 give better results for the three values. Table IV-6 compares the three integration methods to each other with and without instability suppression. The instability suppression has a more noticeable effect on the Euler and Modified

Table IV-5. Computational Time and Accuracy for the Runge-Kutta Integration as a Function of the Integration Time Increment (Δt).

Δt	Normalized Accuracy	Normalized Computational Time
-.0001	*	*
-.005	*	*
-.01	*	*
-.05	2.79	36.17
-.1	1.59	17.86
-.5	.14	3.19

* indicates that the total computational time was larger than that allowed for this analysis.

Table IV-6. Comparison of Integration Solution Methods For Δt = -.5.

Solution Method	Normalized Accuracy	Normalized Computational Time	Normalized Weights of Time & Accuracy
Runge-Kutta	.14	3.19	3.33
Runge-Kutta (Instability Suppression)	.14	3.23	3.37
Modified Euler	.07	2.91	2.98
Modified Euler (Instability Suppression)	.17	2.23	2.40
Euler	0	.08	.08
Euler (Instability Suppression)	.10	7.77	7.87

Euler routines. If computational time and accuracy are weighted equally as in Table IV-6, then the Euler algorithm accomplishes the desired results most efficiently.

The exponential acceleration of integration solutions is discarded for this system because the transient solution is not approximated by an exponential very well. As a result, the solution either goes unstable or requires a prohibitive amount of computation time if the instability suppression is included.

The linearly accelerated integration algorithms are sensitive to the value of the constant of proportionality used to accelerate the soltuion. If this constant is chosen too large, this procedure will also result in unstable solutions or prohibitive computation times if instability suppression is used. Table IV-7 provides a comparison of some solutions to Equation (IV-29) obtained by Euler integration and linearly accelerated Euler integration. The linearly accelerated routine produces slightly better results than the simple Euler integration routine. For a particular system, a value for the constant proportion adjustment can be obtained empirically. This must be done to minimize the possibility of unstable solutions.

For all solution techniques considered, Table IV-8 presents those algorithms requiring the least computational time, Table IV-9 presents those techniques giving the most accurate solutions, and Table IV-10 presents the best solution methods for an equal weighting of time and accuracy. The Euler integration routine with a step-size of -.5 gives the best results of the algorithms employed to solve the Riccati

Table IV-7. Comparison of Euler Integration and Linearly Accelerated Euler Integration Solutions to the Riccati Equation.

Algorithm	Δt	Normalized Accuracy	Normalized Computational Time	Equal Weighting of Time and Accuracy
Euler	-.1	1.01	3.54	4.55
Euler	-.05	2.98	8.22	11.19
Euler	-.01	29.65	34.58	64.23
Acc Euler	-.1	.08	3.05	3.14
Acc Euler	-.05	1.93	2.51	4.43
Acc Euler	-.01	32.04	12.41	44.44

Table IV-8. The Solution Methods Requiring the Least Computational Time.

Algorithm	Δt	Normalized Computational Time
Potter's Algebraic	*	0
Euler	-.5	.08
Euler (Linear Acceleration)	-.1	1.65
Modified Euler	-.5	2.23
Euler (Linear Acceleration)	-.05	2.51
Runge-Kutta (for comparison)	-.5	3.19

* An Algebraic Technique

Table IV-9. The Solution Methods Resulting in the Best Accuracy.

Algorithm	Δt	Normalized Accuracy
Euler	-.5	0
Modified Euler	-.5	.07
Euler (Linear Acceleration)	-.1	.08
Euler (Instability Suppression)	-.5	.10
Runge-Kutta	-.5	.14
Kleinman Iterative	*	.17

* Algebraic Algorithm

Table IV-10. The Solution Methods Providing the Best Tradeoff Between Time and Accuracy.

Algorithm	Δt	Normalized Weighting of Accuracy and Comp Time
Euler	-.5	.08
Potter's Method	*	.95
Euler (Linear Acceleration)	-.1	2.22
Modified Euler	-.5	2.40
Euler (Linear Acceleration)	-.05	3.28

* Algebraic Algorithm

equation. Table IV-11 compares the two algebraic techniques with the Euler integration solution because the integration solutions have the property that the numerical solution goes unstable if the step-size is chosen to be too large. In contrast, larger step-sizes give better accuracy and computational time trade-offs. This is not true for the algebraic techniques so that, depending on the application, it may be desirable to use the less efficient algebraic algorithms.

Table IV-11. Algebraic Techniques Compared With the Euler Algorithm With $\Delta t = -.5$ and the Runge-Kutta Algorithm With $\Delta t = -.5$.

Algorithm	Normalized Accuracy	Normalized Computational Time	Normalized Accuracy and Time Weighting
Runge Kutta	.14	3.19	3.33
Euler	0	.08	.08
Potter's Method	.95	0	.95
Kleinman Iterative	.17	15.76	15.94

V. SIMULATION RESULTS

Simulation results are presented in this chapter to compare the basic CMG steering laws presented in Chapter III with the total optimal CMG control law presented in Chapter IV. The system parameters used in these simulations are those used in [7].

It is stated in Chapter III that the three basic steering laws presented there require a controller that provides a commanded torque as an input to these steering laws. Since these basic steering laws are compared to the total optimal control law, the torque commanded by the controller will be determined from optimal control considerations. These conditions should provide a fair comparison of the system responses.

The control law that gives the commanded torque for the basic steering laws is developed in a manner analogous to that used to develop the total optimal control law in Chapter IV. Equation (IV-27) again describes the performance measure, but the terms in the performance measure refer to different variables. The sixth order state vector is composed of the vehicle attitude errors and attitude rate errors while the control vector is the torque command vector. The R matrix is chosen as the identity matrix while the Q matrix relatively weights the elements of the state vector as well as relatively weighting the state vector with control effort expenditure. Linearizing the

state equations about the commanded vehicle attitude and the nominal vehicle rates puts this problem in the form of the linear regulator problem as in Chapter IV. The resulting optimal control torque is linear negative feedback of the position and rate errors. If a particular response is desired, the closed-loop system matrix may be examined and varied by varying the state feedback to obtain the desired closed-loop eigenvalues since the optimal law is known to be constant negative feedback of the states. This approach will result in the desired response without being concerned with the problem of determining the weighting matrices to give this response.

The partitioned inverse steering law described by Equation (III-19) and the pseudoinverse steering law described by Equation (III-23) are both open-loop steering laws. (Algorithms for computing the pseudoinverse are given in [15]). As a result, these steering strategies do not consider the CMG cross-coupling effects. Consequently, the system using these steering laws goes unstable as shown in Figure V-1. This response is typical for both of these open-loop steering laws.

These steering laws are modified by negatively feeding back the actual torque on the vehicle to force the basic steering law to create a torque that more closely follows the commanded torque. This negative feedback may be implemented by using the measured gimbal angles and gimbal rates to compute the actual torque using

$$\vec{T} = D\vec{\delta} + E\vec{\Omega} \qquad \text{(V-1)}$$

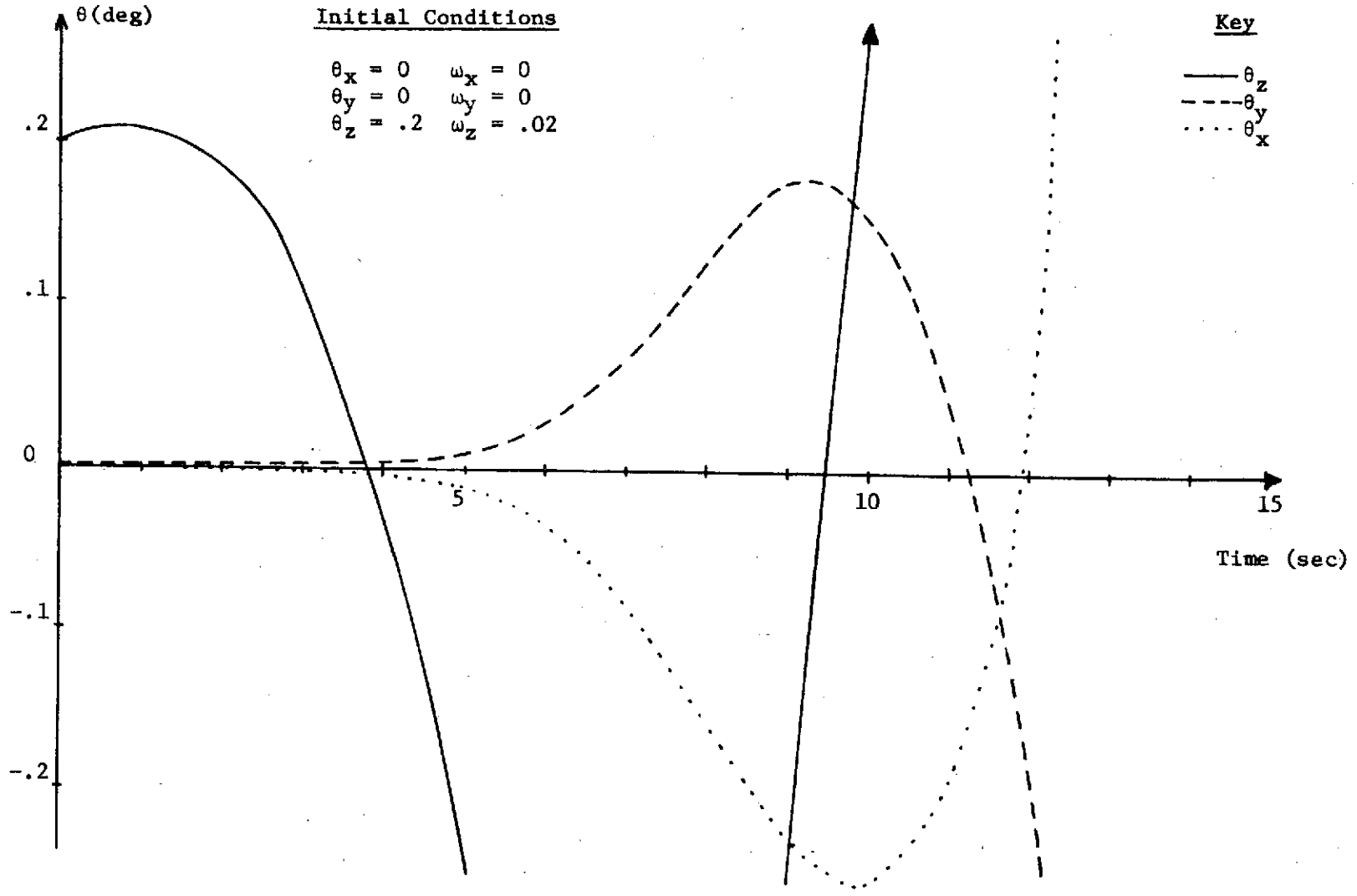

Figure V-1. Basic open-loop steering law response for an initial error in one axis only.

since D and E are both functions of the gimbal angles only. Implementing this negative feedback has the advantage of decreasing any detrimental cross-coupling effects as may be observed in Figures V-2 and V-3. Figures V-2 through V-5 present the responses of the different systems to initial position and rate errors in one axis only. The cross-coupling effects for the control laws may be compared to one another by examining the axes that had no initial errors in them.

Figure V-6 compares the responses of the four systems to an initial position and rate error in one axis only. The other axes are not included in Figures V-6 through V-11 because Figures V-2 through V-5 have illustrated how small the cross-coupling effects are. The pseudoinverse steering law and the optimal steering law give almost the same response. This response is underdamped, but faster than the partitioned inverse steering law and the total optimal CMG control law. The partitioned inverse steering law gives an overdamped response that is faster than the total optimal control law but slower than the other two steering laws. This partitioned inverse steering law gives the best response for the weighting matrices chosen in these cases. The response of the total optimal CMG control law is similar to the partitioned inverse steering law, but it is slower in achieving the desired control. Figures V-7 through V-11 compare the responses of the four systems to one another for initial errors in two axes and three axes. Examination of these cases reveals that the same comments apply to them that applied to Figure V-6.

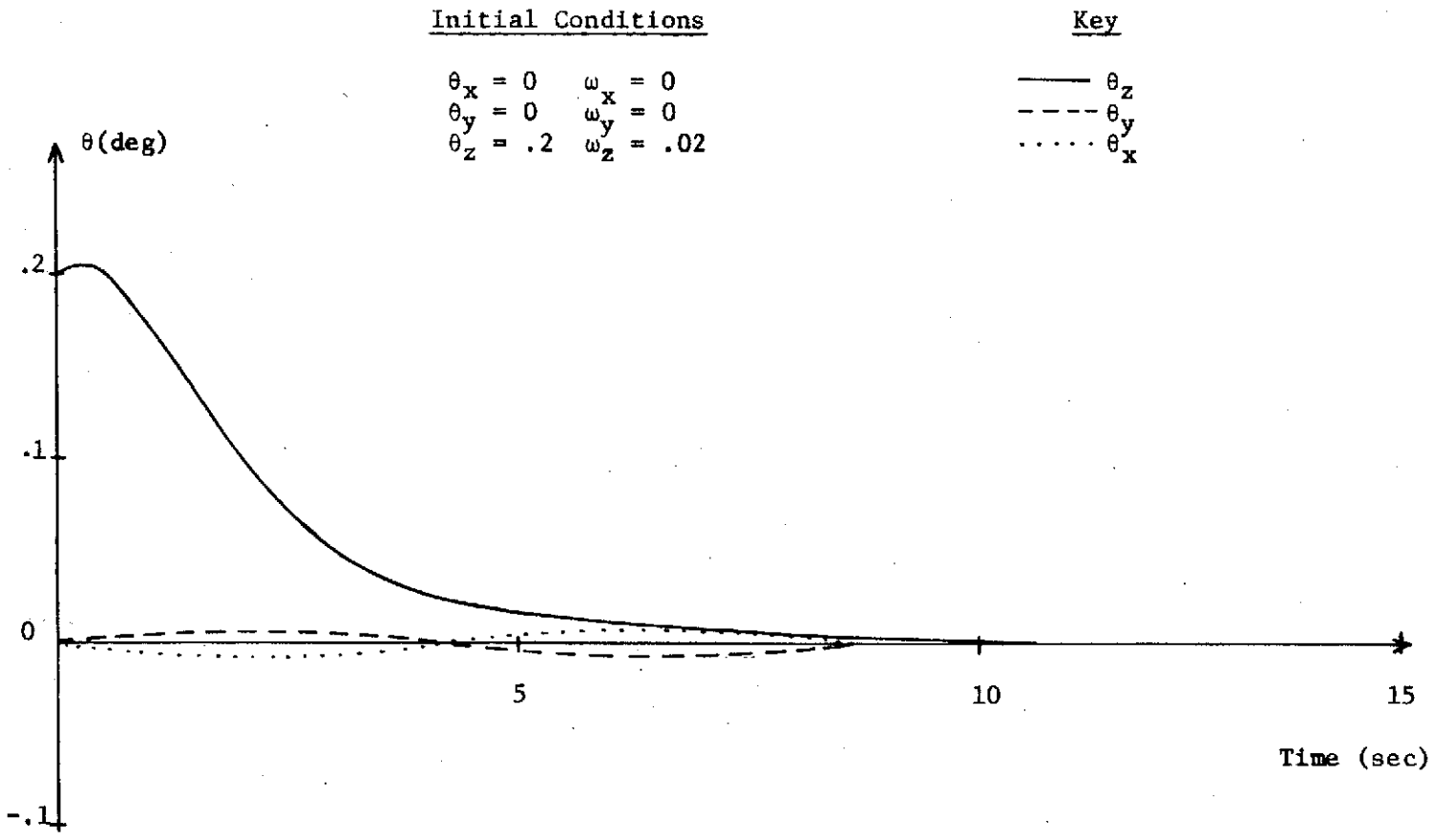

Figure V-2. Attitude vs. Time for an initial error in one axis using the partitioned inverse steering law.

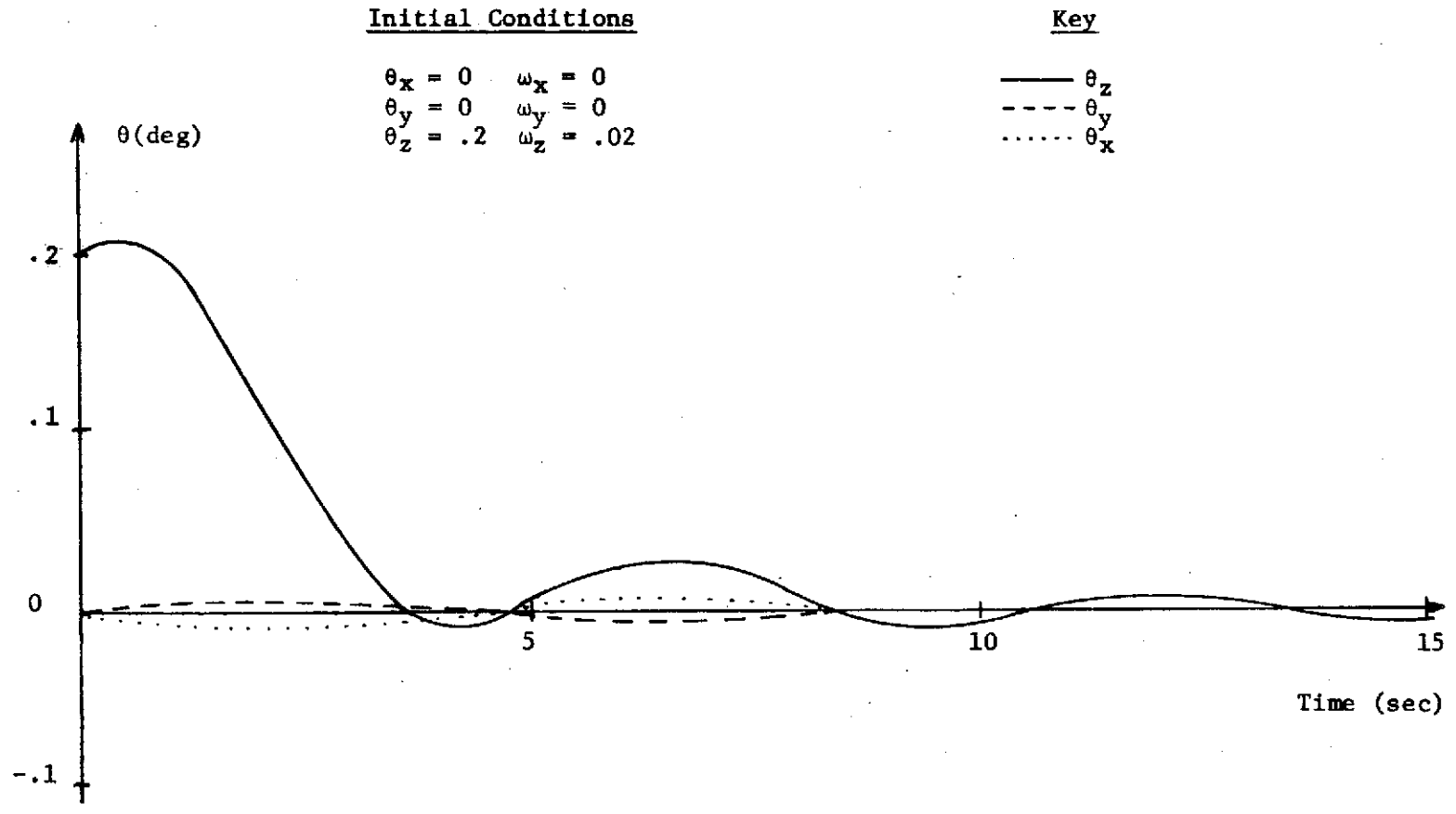

Figure V-3. Attitude vs. Time for an initial error in one axis using the pseudoinverse steering law.

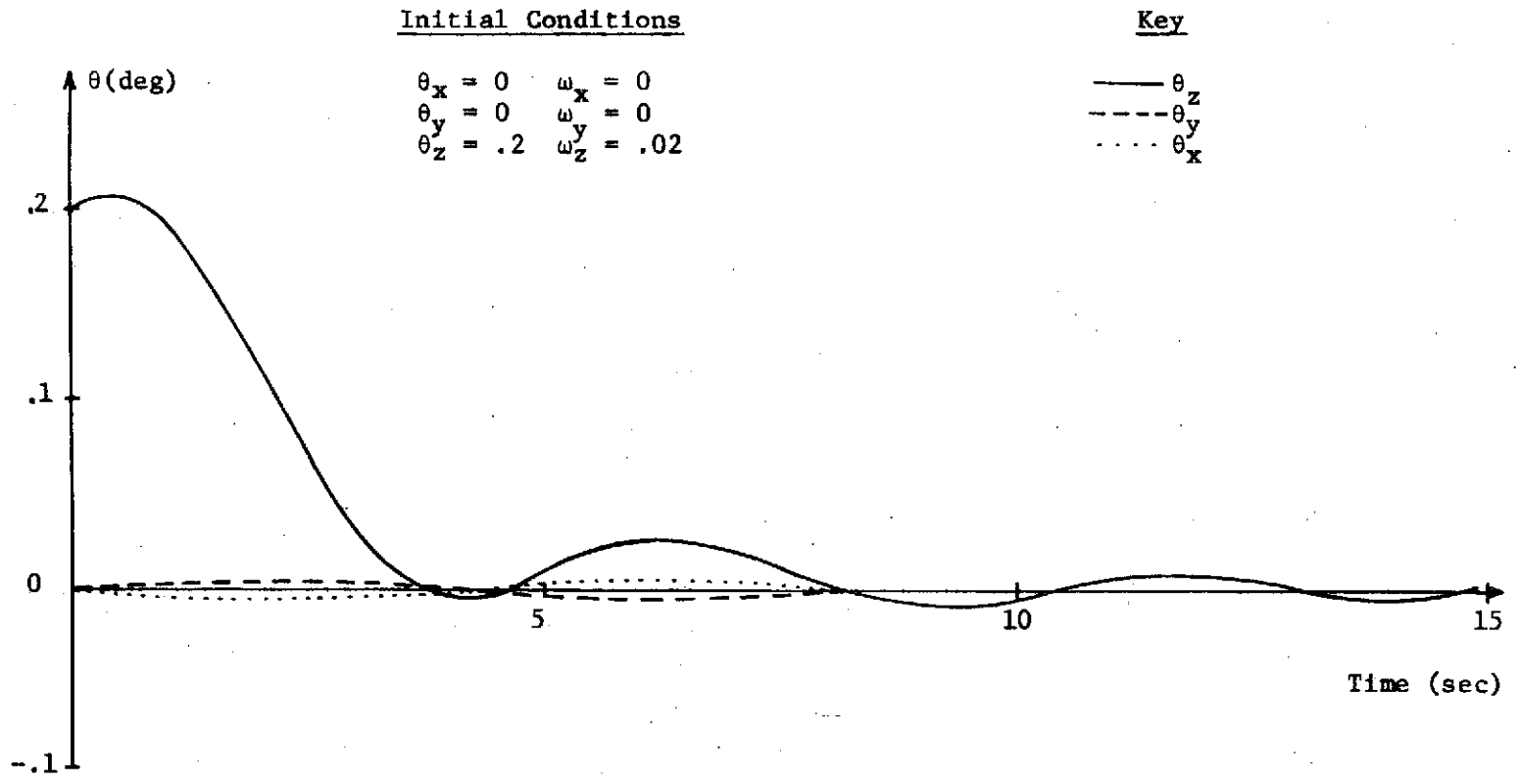

Figure V-4. Attitude vs. Time for an initial error in one axis using the optimal steering law.

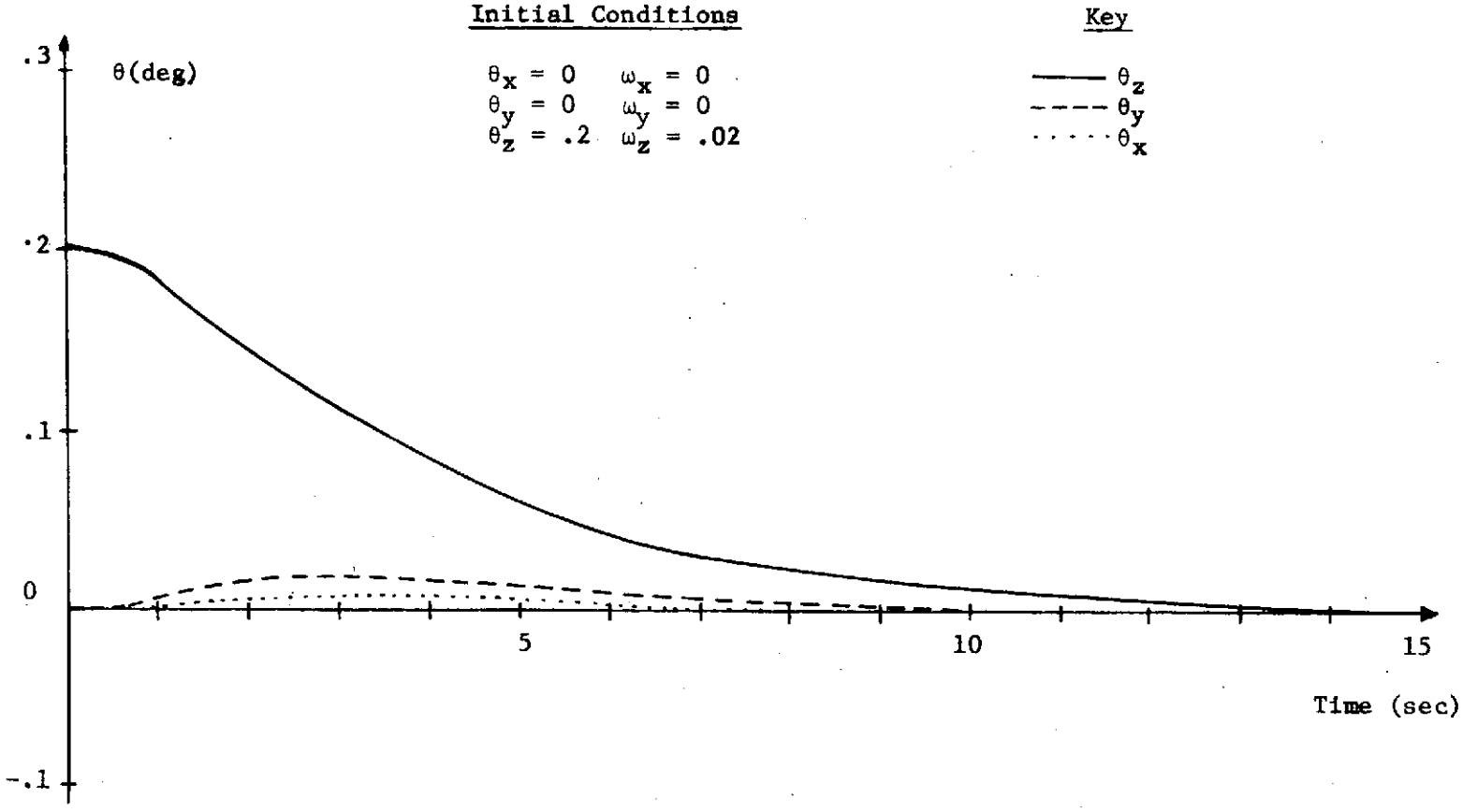

Figure V-5. Attitude vs. Time for an initial error in one axis using the total optimal CMG attitude control law.

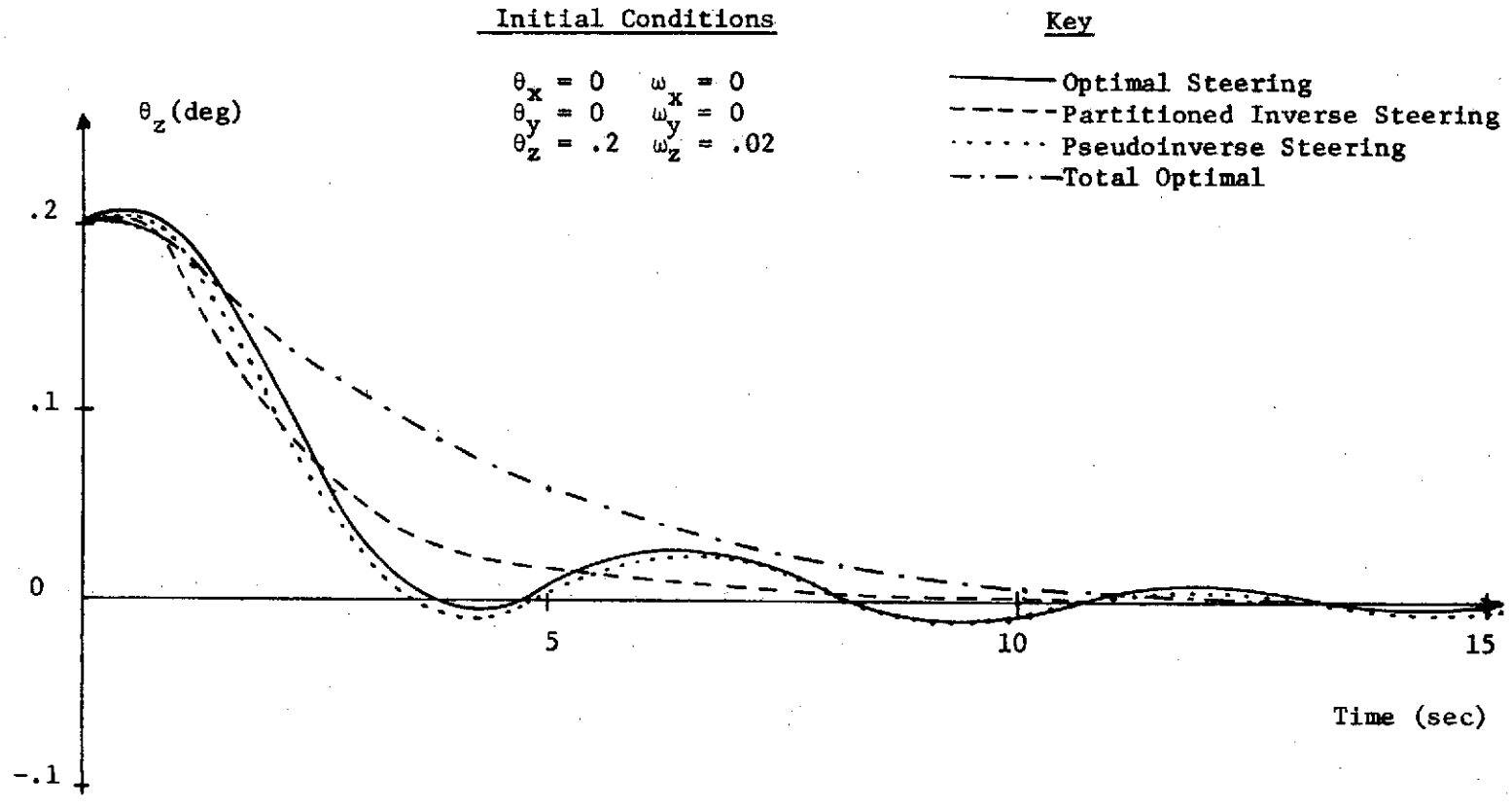

Figure V-6. Comparison of the four CMG control laws for an initial error in one axis.

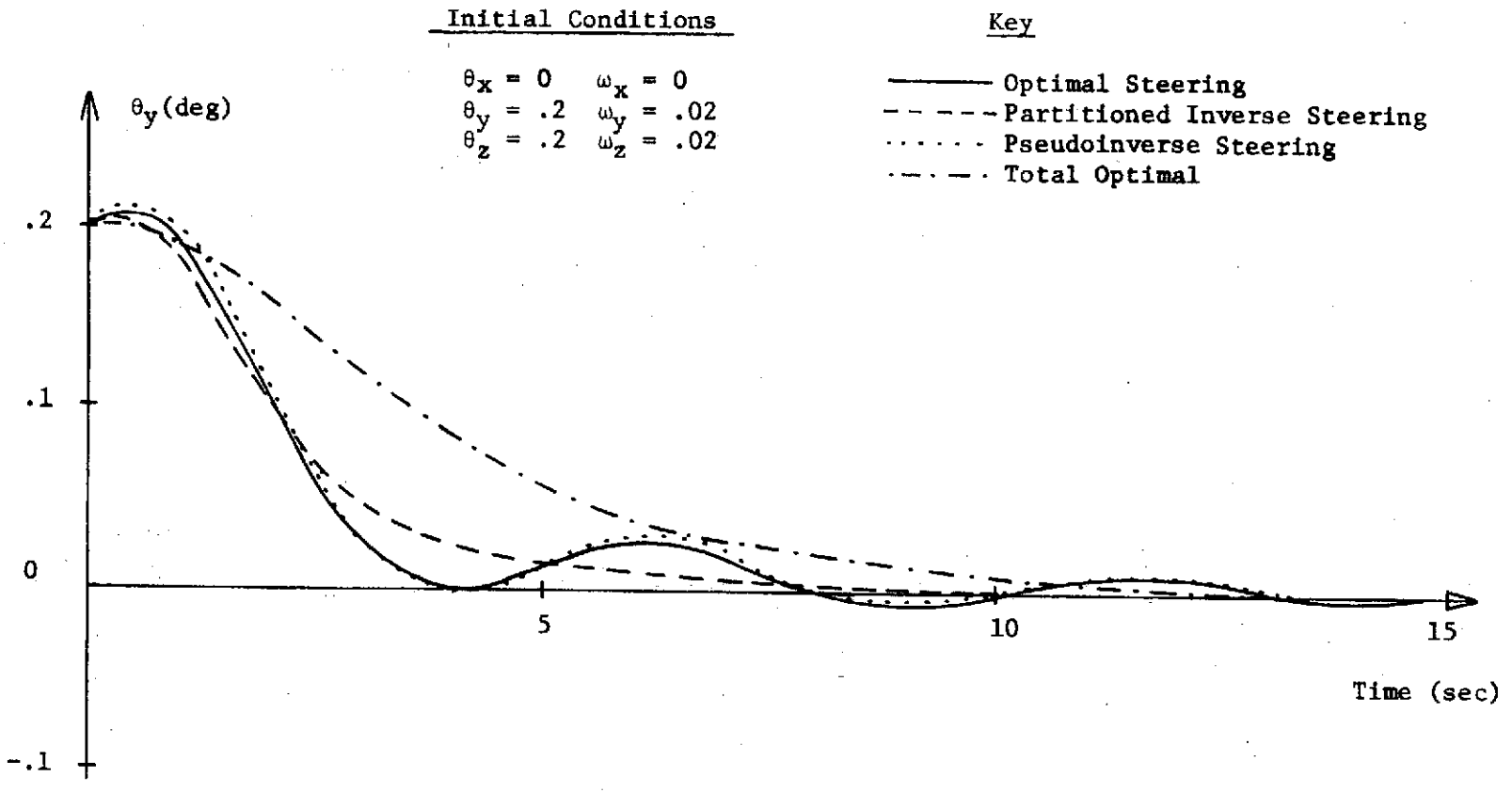

Figure V-7. Comparison of the four CMG control laws for an initial error in two axes.

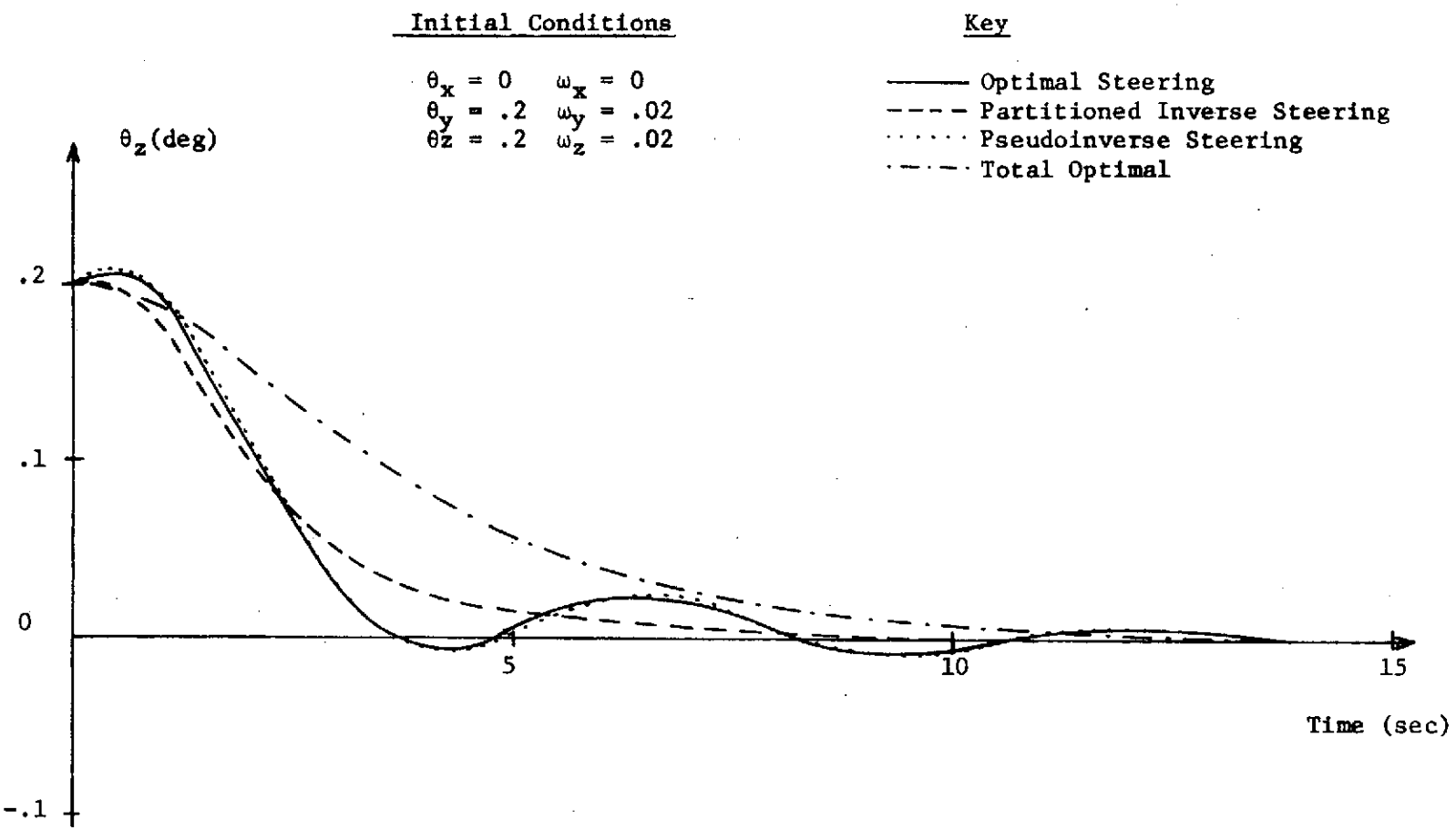

Figure V-8. Comparison of the four CMG control laws for an initial error in two axes.

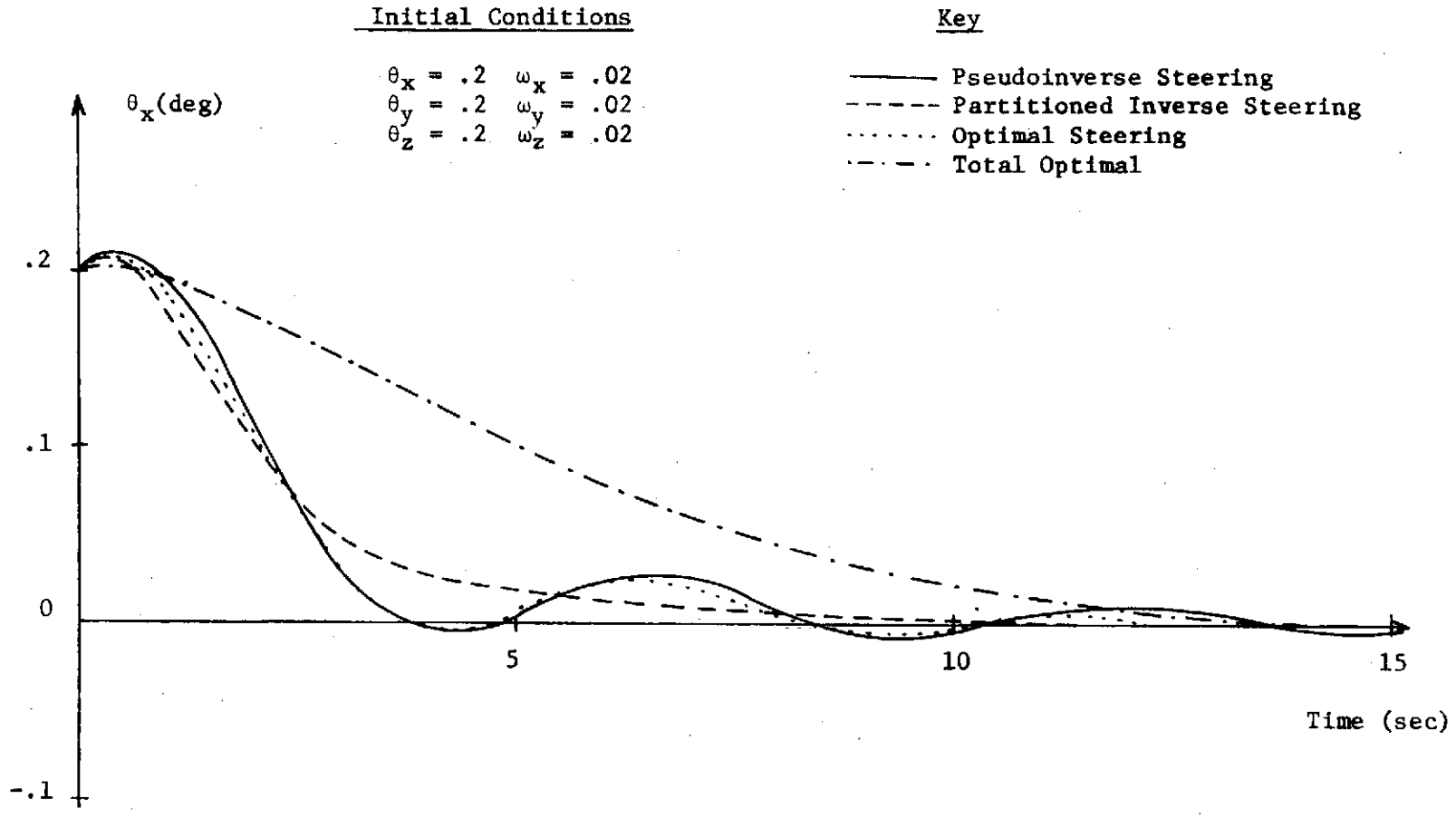

Figure V-9. Comparison of the four CMG control laws for an initial error in three axes.

C-2

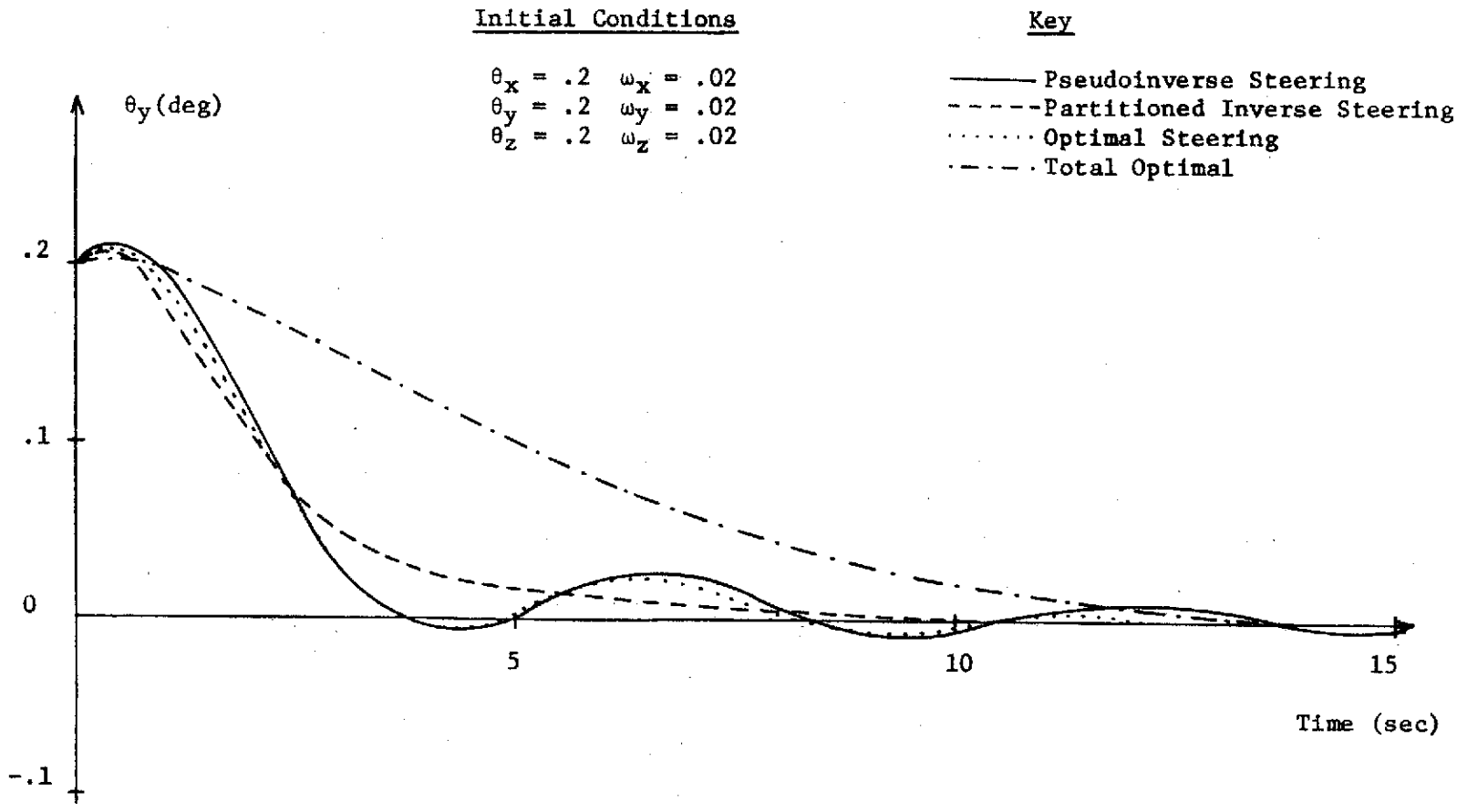

Figure V-10. Comparison of the four CMG control laws for an initial error in three axes.

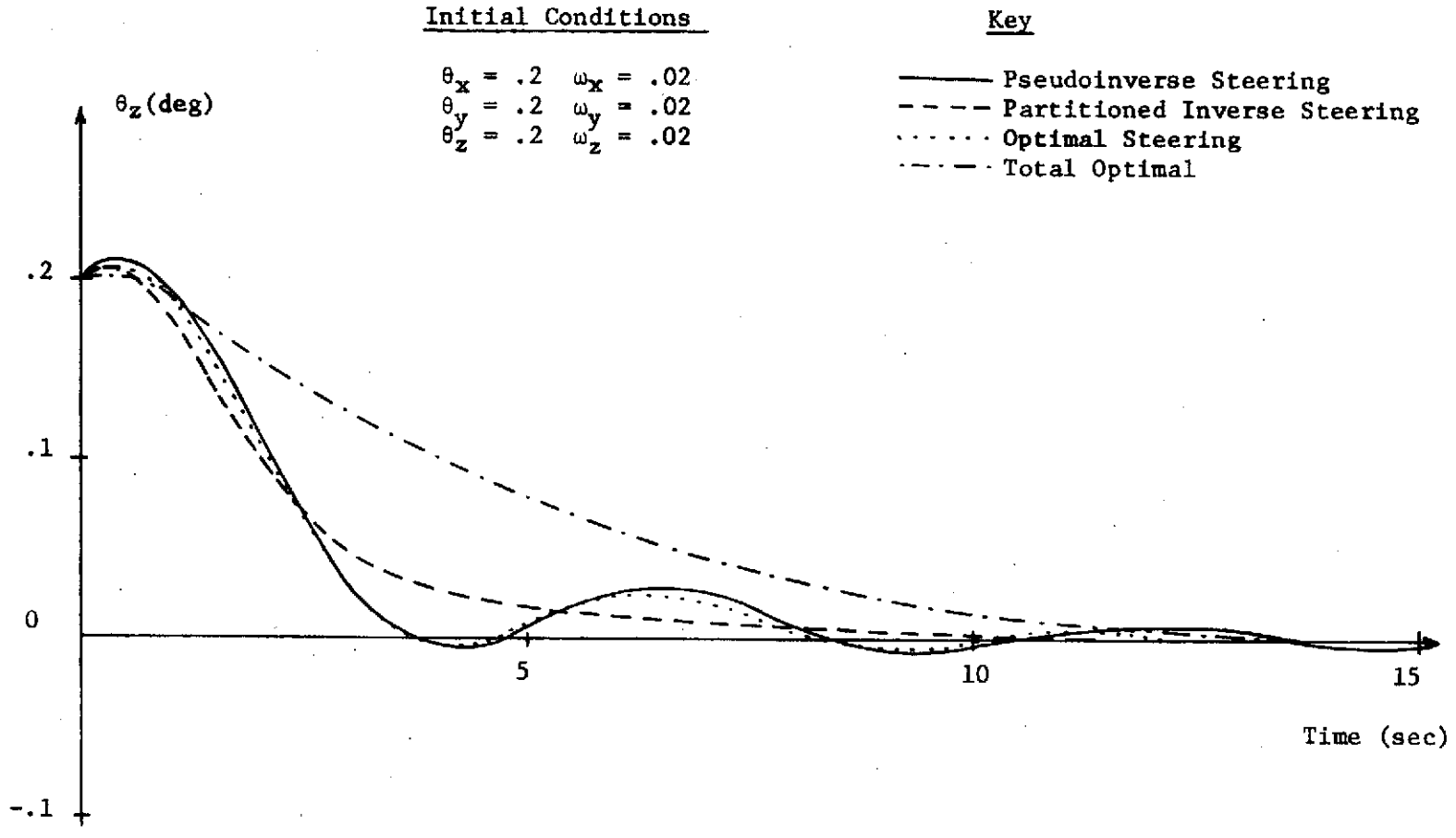

Figure V-11. Comparison of the four CMG control laws for an initial error in three axes.

These results are not presented to imply that one of these systems is better than the other in an absolute sense. The responses of these systems may be varied by changing the relative weightings of some of the parameters. The partitioned inverse steering law and the pseudoinverse steering law will have different responses only if the relative weighting of vehicle position and rate errors against control effort is changed in the development of the vehicle control law. The optimal steering law response may be varied by changing the relative weighting between the gimbal rates and the torque error in the development of the optimal steering law. It may also be varied by changing the vehicle control law as for the other steering laws. The response of the total optimal CMG control law may be changed by changing the relative weighting of position and rate errors of the vehicle against the commanded gimbal rates. Keeping in mind this possibility of varying these responses, the main point to be made by these simulation results is that the basic steering laws with an optimal vehicle control law can control the vehicle as well as the total optimal CMG attitude control law. Furthermore, these basic steering laws are implemented without the computational problems associated with the total optimal control law. It is suggested that future investigations compare and analyze these systems in more detail.

REFERENCES

[1] Donald E. Kirk, Optimal Control Theory, Prentice-Hall, Englewood Cliffs, New Jersey, 1970.

[2] Louis A. Morine and Bernard J. O'Connor, "The Description of the CMG and its Application to Space Vehicle Control," The Bendix Corporation Pub. No. 674-7, February 20, 1967.

[3] Charles H. Ross, "Antisingular Optimal Control of Control Moment Gyros," Northrop TR-795-9-548, May, 1969.

[4] Donald M. Wiberg, State Space and Linear Systems, McGraw-Hill, New York, N. Y., 1971.

[5] Charles H. Ross, "A Proposed Total CMG Attitude Control System for Orbiting Spacecraft," Northrop M-795-9-643, October, 1969.

[6] R. E. Kalman, "On the General Theory of Control Systems," Proceedings of First IFAC Congress, pp. 481-493, International Federation on Automatic Control, 1960.

[7] R. E. Skelton, "Optimal Momentum Management in Momentum Exchange Control Systems for Orbiting Vehicles," Sperry Rand Report No. SP-230-0252, September 2, 1969.

[8] R. E. Skelton, "Optimal Momentum Management in Momentum Exchange Control Systems for Orbiting Vehicles," Thesis, University of Alabama, 1969.

[9] David L. Kleinman, "An Iterative Technique for Riccati Equation Computations," Bolt, Beranek, and Newman Inc. Technical Memorandum No. DLK-1, June 30, 1970.

[10] M. Jamshidi, G. C. D'Ans, and P. Kokotović, "Application of a Parameter-Imbedded Riccati Equation," IEEE Transactions on Automatic Control, pp. 682-683, December, 1970.

[11] David J. Russell, "Computer Program to Accelerate Transient Finite-Difference Solutions to Steady-State," Third Annual Houston Conference on Computer and System Science, pp. 291-301, 1971.

[12] David L. Kleinman, "On an Iterative Technique for Riccati Equation Computations," IEEE Transactions on Automatic Control, pp. 114-115, February, 1968.

[13] T. E. Bullock and C. E. Fosha, "A General Purpose Program for Estimation, Control, and Simulation," Proceedings of Eighth Annual IEEE Region III Convention, Huntsville, Alabama, pp. 102-107, November 19-21, 1969.

[14] J. Potter, "Matrix Quadratic Solutions," SIAM Journal on Applied Mathematics, Vol. 14, No. 3, May, 1966.

[15] S. Barnett, Matrices in Control Theory, Van Nostrand Reinhold, London, England, 1971.